2

Thermomechanical Characterization of Shape Memory Alloy Materials

D. J. Hartl and D. C. Lagoudas

Having introduced the fundamentals of shape memory alloy behavior, the characterization of SMA materials is discussed here. Such a discussion fosters a better understanding of the thermomechanical constitutive response of SMAs. Furthermore, proper determination of required material properties is necessary for the development of comprehensive and accurate SMA material models. Finally, it is perhaps the most important step in the practical implementation of SMAs. Whatever methodology one uses to design a given SMA application, a quantitative evaluation of key material properties is required.

2.1 Introduction

The thermomechanical characterization of an SMA provides a qualitative demonstration of the material behavioral characteristics and allows one to derive distinct quantitative material properties. Like other classes of structural materials, shape memory alloys are tested by subjecting specimens to prescribed thermomechanical inputs while monitoring the exhibited material response. However, though the characterization of SMAs is based on the same principles used to test other material systems, unique considerations exist due to the complex constitutive behavior of shape memory alloys. These issues will be this chapter's focus.

SMAs exhibit coupled thermomechanical behavior, requiring the experimentalist to carefully consider the particular inputs, or *loading paths*, applied to the material. To quantify the complex behavior of SMA materials, various loading paths are imposed while phenomena associated with the phase transformation are recorded. These phenomena include the shape memory effect and pseudoelasticity, as discussed in the first chapter. This chapter will focus on the application and measurement of three thermomechanical fields in particular: stress, strain and temperature. As will be explained in the following chapter, either histories of stress and temperature or strain and temperature will be prescribed while the evolution of the third quantity will be measured, usually by appropriate interpretation of traction, displacement, and temperature measurements at the specimen boundary. To consistently characterize an

D.C. Lagoudas (ed.), *Shape Memory Alloys*, DOI: 10.1007/978-0-387-47685-8_2,

SMA material in a manner that suitably determines its properties, it is useful to establish an experimental process during which various loading paths are applied in a carefully considered progression. Such a process will be proposed in this chapter and will be illustrated by considering the actual testing of various SMA specimens.

2.1.1 Review of SMA Characterization Methods

From the time of the first comprehensive studies published on shape memory alloy properties, particularly with respect to NiTi [1], researchers have sought to fully understand the behavior of these materials. Many of the phenomena observed in SMAs can now be explained in terms of underlying microstructural mechanisms and SMA behavior, under a given thermomechanical loading path, can be phenomenologically described as this current level of knowledge has matured over several decades. This has been made possible by carefully planned and executed experimentation.

Years after the initial well-published discovery at the Naval Ordnance Laboratory, NASA scientists completed a comprehensive report on the properties of Nitinol [2]. This report presents information regarding crystallography, processing techniques, physical, mechanical and chemical properties, and potential applications. Since that time, experimental investigation has been ongoing. Researchers further focused on understanding the metallurgical and microstructural aspects of shape memory and pseudoelastic behavior as exhibited by a number of different alloy systems [3–6]. Experimental research then began to focus on the phenomenological aspects of SMA behavior, including increased investigation of the exhibited thermomechanical coupling and the engineering applications of SMAs [7–13].

As shape memory alloy materials have gained acceptance for use in specialized engineering applications, it has become clear that some testing methods should be standardized, especially in the medical field. ASTM International has addressed this need by publishing standard test methods to guide SMA experimentation efforts, especially for research and development of applications. While some standards are restricted to the definitions of terms or the suitable composition of NiTi alloys [14, 15], others address experimental methods directly. Standard test method F-2004 [16] addresses the details of Differential Scanning Calorimeter (DSC) testing. As shown in Chapter 1, this is an important test for observing transformation behavior in SMAs under zero stress (see Sect. 1.8) and is used as a guideline to derive an estimate for all four key transformation temperatures (i.e., M_s, M_f, A_s, and A_f). Note that some special equipment is required and will be shown in later sections.

As an alternative method to estimate austenite start and finish temperatures (A_s and A_f) only, specification F-2082 [17] recommends the "Bend and Free Recovery" test. This specification makes direct use of the shape memory effect (Sect. 1.4) and does not require specialized equipment. According to the specification, a specimen (wire, tube, or strip) is deformed when bending at

a low temperature ($T < A_s$), causing regions to form detwinned martensite. This leads to the generation of transformation strains that are not recovered upon unloading due to the test temperature being below A_s. The sample is then slowly heated, and its geometric configuration is monitored. The temperature at which the sample begins to recover its initial shape is declared to be approximately equal to A_s, and the temperature at which recovery is completed is declared to be approximately equal to A_f. In addition to the martensite to austenite ($M \leftrightarrow A$) transformation, this specification also addresses martensite to R-phase to austenite ($M \rightarrow R \rightarrow A$) transformation for materials that exhibit this behavior (Sect. 1.8). The bend/free recovery method is not addressed further here, but should be considered as a qualitative method of measuring two of the four transformation temperatures.

Finally, specification F-2516 [18] addresses the tensile testing of SMA specimens, especially those exhibiting pseudoelasticity at room temperature (see Sect. 1.5). Applying mechanical loading/unloading cycles is important in the testing of many materials, but for the investigation of SMAs, this is a key step. The parameters described in this specification, such as *upper plateau strength* and *lower plateau strength*, will be shown to correspond to the characterization methods presented in this chapter. The scope of the ASTM standards is a basic understanding of certain aspects of SMA behavior, mostly relevant to medical applications, and is not the full thermomechanical characterization of these materials. Furthermore, they are not intended to calibrate phenomenological models such as those described in Chapter 3. These complex efforts require additional considerations as discussed throughout the remainder of this chapter. As new constitutive models are being developed for SMAs, additional tests are necessary for providing material parameter inputs.

Clearly, the methods and processes presented in this chapter derive directly from decades of previous experimental work performed by many skilled individuals and research teams. The contribution of this text is simply to summarize and organize various experimental techniques into a comprehensive method by which one can deduce the material properties of interest. Furthermore, aspects of experimentation that have challenged others in the past will be addressed.

2.1.2 Shape Memory Alloy Specimens

To begin the discussion of thermomechanical SMA material characterization, it is appropriate to provide examples of the actual material specimens designed for testing. The reader is assumed to have some familiarity with the experimental systems used to provide the necessary loads (experimental inputs) and to monitor material responses. Although there are unique experimental considerations imposed by the behavior of shape memory alloys, such discussion is reserved for Sect. 2.4. This introductory material should be familiar to those who are experienced in experimental material thermomechanical testing.

The most common materials testing performed on SMAs involve tensile axial loading. While the potential configuration of SMA specimens is as varied as those of other metallic material systems, the manner in which SMAs are utilized does motivate the commonality of particular specimen forms. For example, many SMA applications use wire components because they provide relatively high tensile forces and displacements in a compact and simple configuration. Therefore, the SMA specimen forms most frequently tested are wire tensile specimens and this form presents the experimentalist with both advantages and challenges. Perhaps the most beneficial aspect of testing wires is that specimens often arrive from the manufacturer in a useable form such as spooled wire as shown in Fig. 2.1. Due to their long and thin configuration, wire specimens provide a simple gauge length over which stresses are homogeneous. However, because the cross section at the ends of a wire specimen is the same as that in the gauge length, prevention of excessive stress concentrations and resulting premature failure at the grips can be challenging. One possible solution to this problem is presented in Fig. 2.1 where a wire specimen and a suitable gripping mechanism are shown. Such a grip configuration allows the testing of a range of wire diameters.

Testing is often performed for wires, however it is also common that SMA components be manufactured in 2-D and 3-D forms for some chosen applications. In such cases, SMA tensile specimens may be fabricated in the common 'dogbone' configuration per standard metal testing methods (i.e., ASTM E8) [19]. This is most easily accomplished when the as-received material is

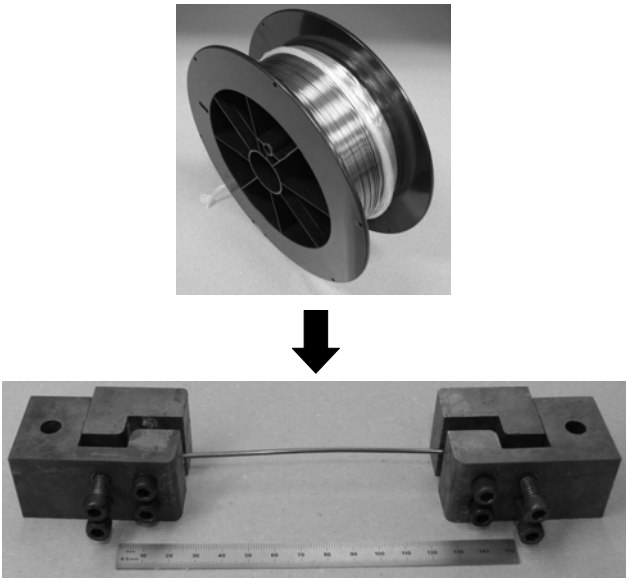

Fig. 2.1. Example of spooled thick NiTi wire and prepared specimen with appropriate grips.

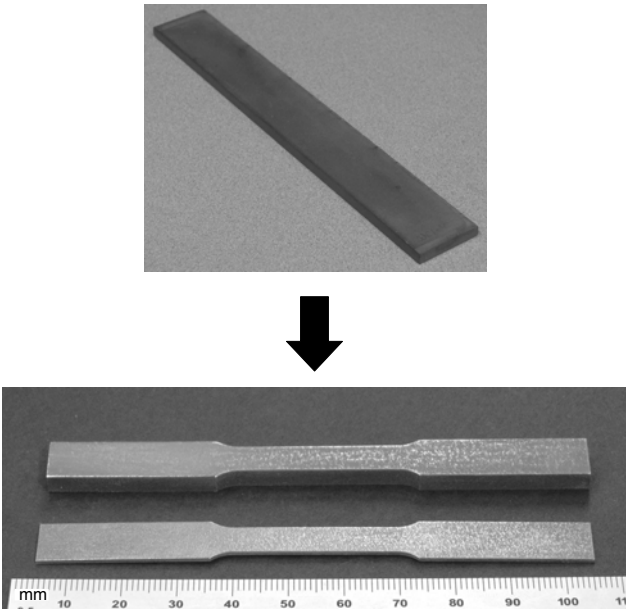

Fig. 2.2. Example of raw Ni60Ti40 (wt.%) plate and subsequent ASTM "dogbone" specimens [19] machined from such plates using EDM.

in plate form. An example of this can be seen in Fig. 2.2 where two NiTi (Ni60Ti40 wt.%) plates of different thickness are shown. It is important to note that due to their thermomechanical behavior, machining SMAs is difficult using current methods. High cutting speeds are necessary for cutting processes that remove material (e.g., drilling and lathing). Methods such as water jet cutting and electrical discharge machining (EDM) are often used as well. EDM is especially useful for machining tensile specimens from different regions throughout properly homogenized bulk material of arbitrary shape. Examples of such a bulk form and the resulting specimens are shown in Fig. 2.3.

Designers and analysts often require information on the compressive behavior of SMAs, which may differ from the complimentary tensile response. For this purpose, compressive specimens are also often required [20, 21]. Though recognized standard protocols (e.g., ASTM standards) for SMA compressive testing do not exist, the general ASTM guidelines for the compressive testing of metals (ASTM E9) provide information on standard specimen configuration and testing methods [22]. Such specimens can also be accurately machined from raw material via EDM, and an example of this is shown in Fig. 2.4.

Finally, it is often necessary to extend the experimental study of an SMA material beyond simple uniaxial loading. To examine the constitutive response under shear or multiaxial loading, SMA specimens in the form of tubes can be

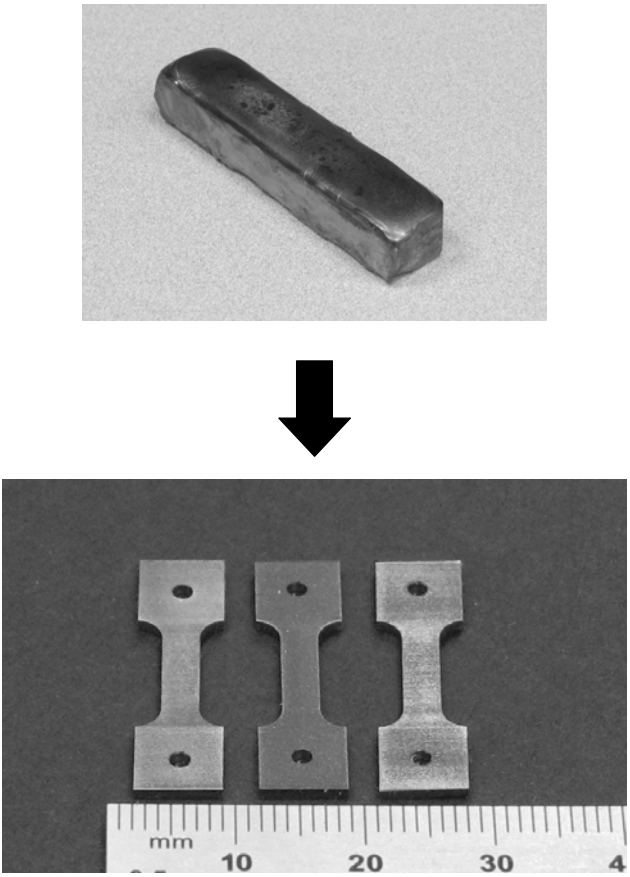

Fig. 2.3. Example of bulk NiTiPd SMA and resulting small SMA "dogbone" specimens machined from its center using EDM.

used. Tubes with sufficiently thin walls (relative to their diameter) provide a region of near-uniform shear stress when subjected to torsion. Response under combined loading can then be assessed if an applied tensile or compressive load is added (compression being applicable for sufficiently short specimens when tested below their buckling load) [23, 24]. Additional application of an internal or external pressure allows consideration of an additional stress state. Example SMA specimens in tube form with varying composition and thickness are shown in Fig. 2.5.

In this section, general aspects of SMA characterization have been discussed. However, to develop an understanding of any material, it is necessary to decide what properties are most useful and then determine under what loading paths these properties are best elucidated. This will be discussed in the following section.

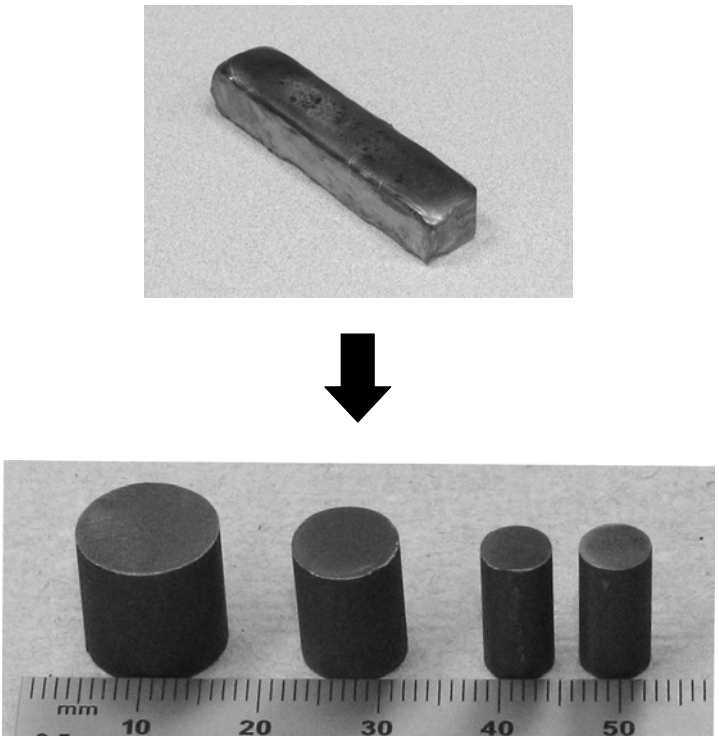

Fig. 2.4. Examples of small NiTiPd SMA compressive specimens EDM machined from the center of bulk raw material. The two specimens on the right follow ASTM E9 specifications [22].

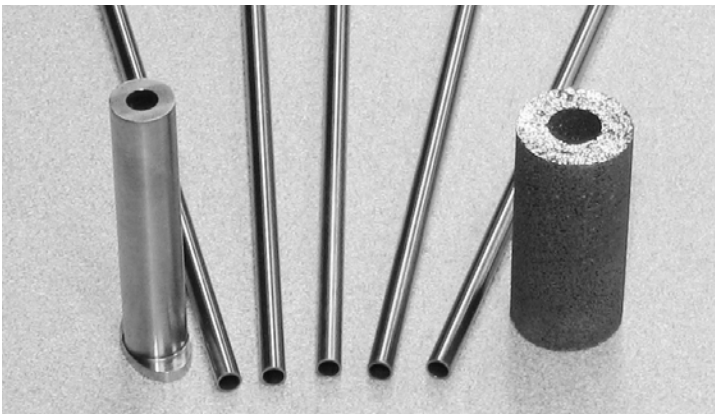

Fig. 2.5. Examples of SMA tube specimens. These include a NiTiPd specimen (left), NiTi high aspect ratio samples (center), and a porous NiTi sample (right).

2.2 Thermomechanical Material Properties of SMAs for Engineering Applications

As it has been discussed in Chapter 1, SMAs represent a specific class of metallic alloys that have two stable solid phases, and by following particular paths in the stress-temperature space, these alloys undergo a transformation from one phase to another. Furthermore, these two phases are distinct in their properties. This transformation can lead to generation and subsequent recovery of strains and cause macroscopic shape changes.

SMAs exhibit nonlinear, hysteretic behavior with a strong thermomechanical coupling. Furthermore, SMAs are highly path-dependent, though the phase transformation itself is not intrinsically loading rate dependent. The thermomechanical coupling, however, can lead to an experimental rate dependence (see Sect. 2.4.3). Each of these aspects leads to experimental complexities, and many of the investigative methods used with other inelastic materials are not completely sufficient to describe the material behavior of an SMA. This section will review the SMA thermomechanical response from an experimental point of view and introduce a general set of material parameters useful in quantitatively describing their constitutive behavior. There are other physical properties that could be experimentally investigated (e.g., electrical conductivity, density, specific heat etc.), but these are not addressed in this chapter. For the interested reader, the comprehensive NASA report provides data on such properties [2], while additional information can be found in more recent compilations of work on SMAs [3, 25].

To examine the thermomechanical engineering properties of shape memory alloys, we first determine what aspects of the material behavior can be parameterized. As an example, we examine the phenomenological response of an SMA specimen undergoing pseudoelastic loading. Recall from Chapter 1 that these experiments are performed by applying prescribed forces (stresses) and temperatures and monitoring exhibited deformations (strains). By considering the unique features of this nonlinear material response (e.g. changes in stiffness, hysteresis, etc.), one can see that a properly chosen set of material parameters is useful in quantitatively describing these most important material behaviors. Note that here the primary interest is in the response of polycrystalline engineering forms of SMA material (e.g. wires, rods, beams etc.), and not the single crystal behavior.

Examination of the new set of experimental pseudoelastic results (uniaxial, tensile) are shown in Fig. 2.6a. The following observations can be made (recalling the discussion in Sect. 1.5):

- During loading:
  - The initial response is nearly linear.
  - At some stress level (σ^{Ms}) the stiffness changes, and a behavior similar to plastic yielding is observed. A 'plateau' is formed.

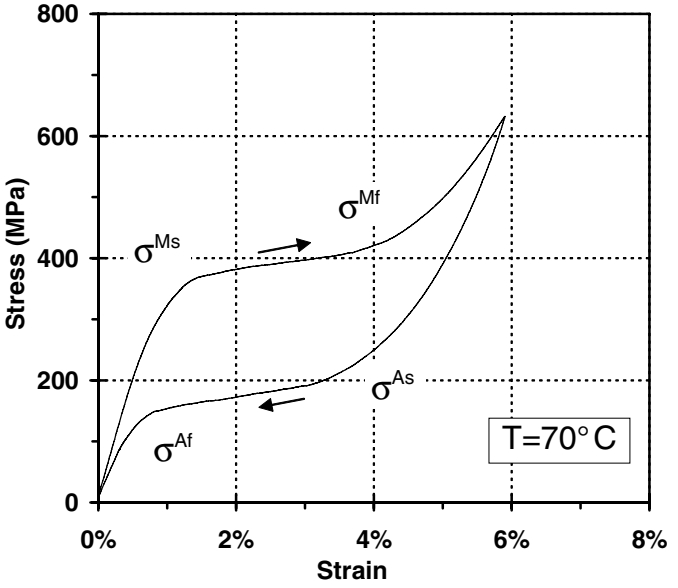

(a)

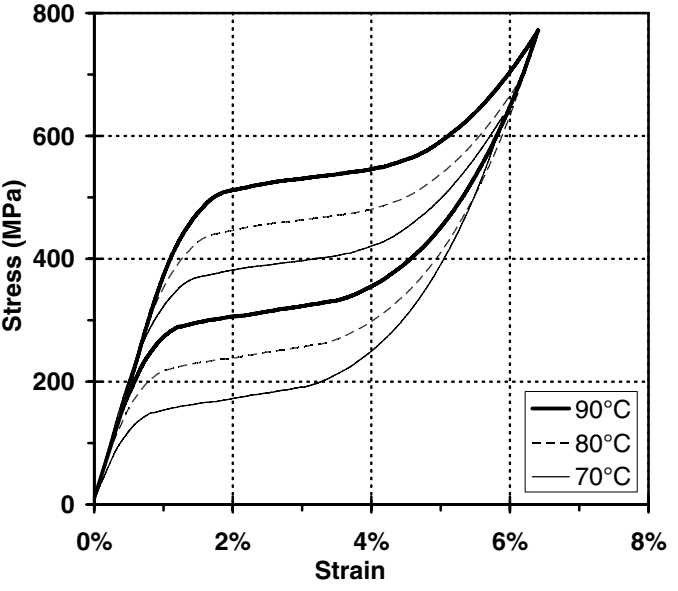

(b)

Fig. 2.6. Experimental example of constant temperature phenomenological transformation behavior in NiTi: (a) single temperature of $T = 70\,^{\circ}\mathrm{C}$, (b) multiple temperatures.

  - As stress increases to a second level (σ^{Mf}), the plateau ends and the response stiffens. A nearly linear response with a slope distinct from the first is observed.
- During unloading:
  - The initial response is nearly linear.
  - A plateau with the same strain length as that observed during loading is formed at a lower stress level (σ^{As}).
  - At the end of the plateau (σ^{Af}), the response stiffens and becomes nearly linear, following the same slope as observed during initial loading.

As explained in Chapter 1, the stiff response at low stress (completely below the loading plateau) corresponds to purely austenitic behavior, while the response at higher stress (completely above the unloading plateau) corresponds to purely martensitic behavior. This indicates the need to consider the independent elastic responses of each phase, and that these responses need not be similar. Such understanding of the elastic response is the first key aspect of SMA characterization.

A second interesting behavior highlights the importance of the current thermomechanical (stress-temperature) state. At the given test temperature, particular stress levels initiate the forward and reverse transformation during loading and unloading, respectively. Furthermore, one can envision a pseudoelastic experiment wherein the same level of force is applied, though at a different temperature (i.e., a different thermomechanical state). Recall that as test temperature increases, the stress needed to initiate each phase transformation (A→M and M→A) increases (see Sect. 1.3). As a result, the response will vary with each change in temperature, as illustrated in Fig. 2.6b.

A third important quantifiable behavior is related to the deformation or strain generated during transformation (plateau region). This represents the amount of macroscopic deformation that can be generated via the underlying microstructural motions and is a clear consequence of the solid-to-solid phase transformation.

The effects discussed above are also observed during thermal transformation at nominally constant stress levels. Engineers are often more interested in the properties of an SMA material as an actuator rather than as a pseudoelastic element. In these cases, constant stress tests are useful in illustrating the three key types of material properties. The strain vs. temperature response during such loading can be seen in the example shown in Fig. 2.7a. Consider first the response at temperatures outside the transformation region (i.e., $T < M_f^\sigma$ and $T > A_f^\sigma$). This behavior is due to thermal expansion, as seen in other metals; this is also a thermoelastic effect (like the linear loading/unloading observed at the beginning and end of pseudoelastic loading).

Second, repetition of such a test at varying stress levels illustrates the relationship between the non-zero stress transformation temperatures and the current stress level, as seen in Fig. 2.7b. This is analogous to varying ambient temperature during pseudoelastic testing.

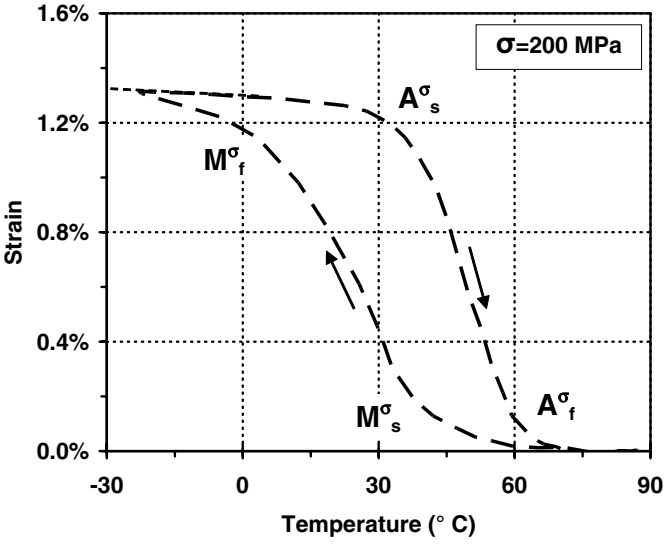

(a)

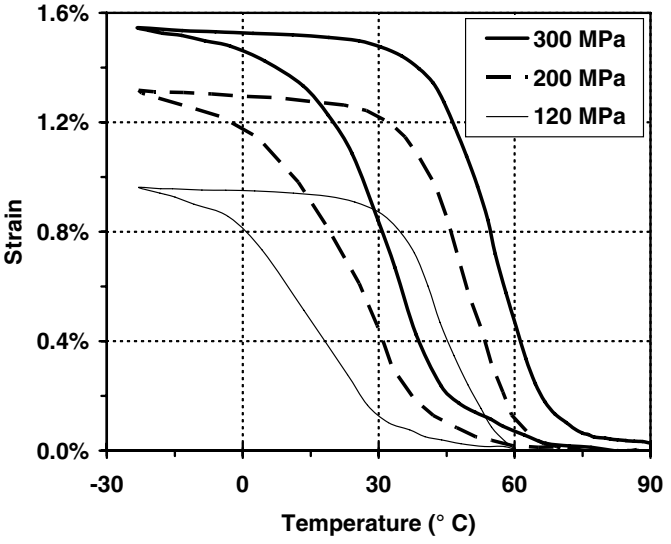

(b)

Fig. 2.7. Experimental example of constant stress phenomenological transformation behavior in NiTi: (a) single stress of 200 MPa, (b) multiple stresses.

Third, note the height of the hysteresis generated during transformation, which represents the amount of inelastic yet recoverable strain being generated and recovered as the transformation evolves.

To review and summarize, we can infer that SMAs require at least three types of material properties to describe three types of behaviors. These types of material properties are:

- *Thermoelastic properties of austenite and martensite* – These parameters, which apply to most structural materials, are necessary to describe the material response when transformation or reorientation is not occurring.
- *Critical stress and temperature states associated with the phase diagram* – These parameters help determine when the process of transformation between phases will begin or end depending on the current thermomechanical state (stress and temperature) and loading history of the material.
- *Transformation strain evolution properties* – These parameters provide a relation between the current state of material transformation (e.g., volume fraction of the various martensitic variants) and the exhibited generation of transformation strain.

2.2.1 Thermoelastic Properties

For each of these three types of properties, one can determine a set of material parameters to sufficiently describe a given shape memory alloy, and we can explore some methods by which they can be found.

Let us first consider the thermoelastic properties. Assuming material isotropy, the elastic stiffness could be represented by the Young's modulus of austenite (E^A), as shown in Fig. 2.8a. The material then transforms into martensite. Once transformation is complete, the fully martensitic material

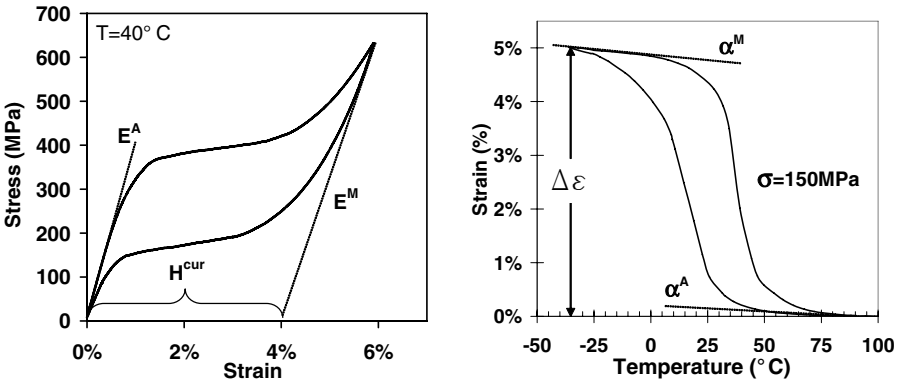

Fig. 2.8. Experimental examples: (a) the pseudoelastic effect, (b) the shape memory effect.

responds elastically once again. Again assuming isotropy, this can be represented by an elastic modulus of martensite (E^M), which is also schematically shown in Fig. 2.8a. These elastic properties can also be found by simple monotonic loading/unloading of the material in a fully austenitic or martensitic state at stresses sufficiently low to prevent transformation or reorientation.

Other elastic properties such as the Poisson's ratio for each phase can be measured concurrently with the stiffness. The coefficient of thermal expansion is used to predict the thermally induced deformation response of pure austenite and pure martensite. This property can be observed in Fig. 2.8b, where constant stress testing is illustrated. Here, the coefficients for austenite and martensite are shown as the slopes of the strain-temperature plots in the fully austenitic and fully martensitic states, respectively.

So, for each phase elastic properties plus the thermal expansion coefficient is required. For design purposes, it is sometimes also useful to characterize the plastic yield and failure behavior of the material. A potential set of thermoelastic properties is as follows:

- The elastic constants of austenite and martensite, respectively. In the case of isotropy, the Young's Moduli, E^A and E^M, and the Poisson's Ratios, ν^A and ν^M, can be used.
- The coefficients of thermal expansion of austenite and martensite, respectively. In the case of isotropy, only two scalar constants, α^A and α^M, are needed.
- Information on the elastic limit of the material. If the material is isotropic, the yield stress of the material in austenite and martensite (σ_Y^A and σ_Y^M) will suffice.

2.2.2 Critical Stress and Temperature States for Transformation (Phase Diagram)

Finally, we review the properties of the phase diagram, which illustrates the stress and temperature conditions for material transformation. Practically this involves the determination of transformation "surfaces," or boundaries of the transformation regions in a stress-temperature space. These indicate where a given transformation (i.e., austenite to martensite or vice versa) begins or ends.

A schematic example of the phase diagram, previously introduced in Chapter 1, is given in Fig. 2.9. The form of these surfaces might be assumed to be linear, quadratic, or otherwise depending on the behavior of the material. Whatever their general form, these four surfaces are partially described by their intersections with the zero-stress axis (i.e., the zero-stress transformation temperatures). However, these temperatures are insufficient to fully describe the configuration of the phase diagram, and additional parameters are needed. A common set of parameters include the slopes of these surfaces at some stress level (e.g., zero stress). Such slopes are known as "stress influence coefficients."

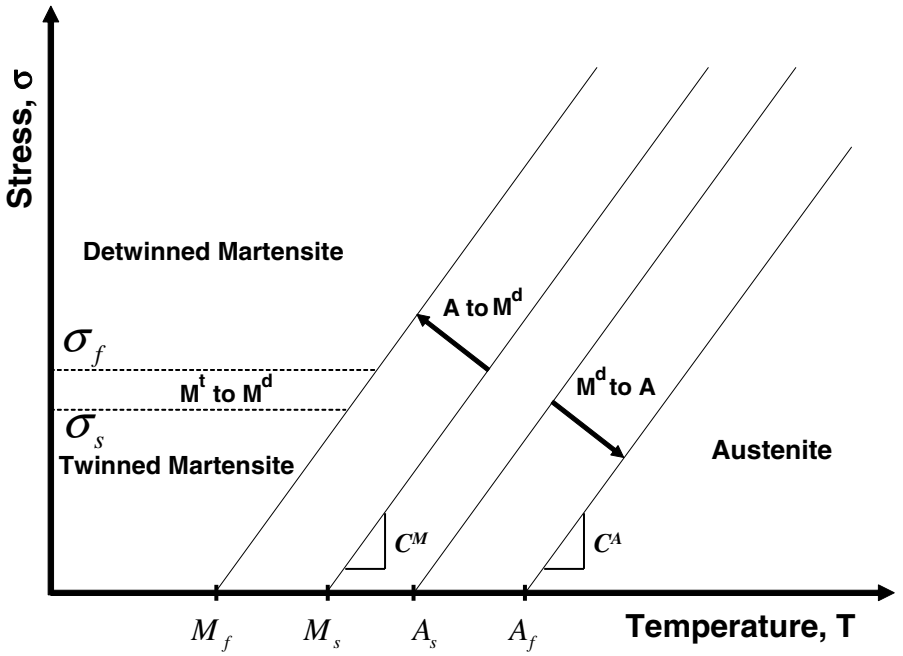

Fig. 2.9. Schematic representation of the phase diagram with possible material properties defined.

Aside from specifying the martensitic phase transformation regions, it is also useful to determine the stresses at which the detwinning of martensite begins and ends. Though this is not technically a transformation but rather a reorientation of martensite, this region can also be plotted on the phase diagram and utilized during design and analysis (see Chapter 6). The parameters required to construct the phase diagram are:

- The initiation and completion temperatures for transformation from austenite to martensite at zero stress (M_s, M_f).
- The initiation and completion temperatures for transformation from martensite to austenite at zero stress (A_s, A_f).
- The *stress influence coefficients* or general slopes of the transformation surfaces. There could be up to four total slopes, though it is often assumed that each pair of surfaces for the two distinct transformations ($A \rightarrow M$ or $M \rightarrow A$) shares a characteristic slope. Thus the zero-stress slopes of transformation regions into austenite (C^A) and into martensite (C^M) are useful parameters, as seen in Fig. 2.9.
- The start and finish stresses for the detwinning of martensite (σ_s, σ_f), which may be temperature-dependent.

2.2.3 Transformation Strain Properties and Hardening

We now continue covering the three key classes of SMA properties by discussing a method to parameterize the generation and recovery of inelastic strains during transformation.

As described in Chapter 1, the formation of martensitic variants from the austenitic parent phase at the microstructural level leads to the observed macroscopic deformation during transformation. However, tracking the detailed configuration of the microstructure (i.e., the evolution of 24 maximum martensitic variants in NiTi) is often beyond the scope of thermomechanical characterization, especially for engineering design and analysis of applications. This would require knowledge of up to 24 internal state variables, for example, which are only observable at length scales much smaller than the engineering scale of thermomechanical testing. Therefore, a more phenomenological approach is often taken whereby the macroscopic deformations are described by a transformation strain field, and the evolution of this field is linked both to the total applied tractions or total applied deformations and to the amount of total martensite present in the material. Theories have been developed wherein the transformation strain dependence on several select variants is considered. Experimentation has supported these theories. Such models will be discussed in Chapter 3 and are addressed in more detail in the literature [26, 27].

When considering the phenomenological behavior of SMAs, one considers the combined effect of microstructural behaviors. In the absence of stresses, local or applied, the martensitic variants form from the parent phase in patterns that lead to negligible macroscopic shape change (i.e., they will self-accommodate). Applied stress results in formation (or reorientation) of preferred martensitic variants, therefore generating observable overall strain due to transformation or detwinning, as discussed in Sect. 1.3. The variant selection is dependent on applied stress, therefore causing the amount of recoverable strain generated to vary with applied stress. Hence, a material parameter to be characterized for SMAs is the maximum strain formed due to transformation at a given stress level and in addition to thermoelastic strains. This strain is the *current maximum transformation strain* and its value depends on several factors, including the crystallography of martensitic transformation, the overall microstructural configuration of grains, texture, configuration and composition of precipitates, in addition to stress level. As a strain measure, the maximum transformation strain could have multiple components. However, for the 1-D experimentation in this chapter, the maximum transformation strain will be considered a scalar quantity given as a function of applied stress for given material conditioning and denoted by $H^{cur}(\sigma)$. If all the martensitic variants are aligned to the maximum extent possible, either due to the effects of applied stress or because of sufficient material training, then the material is said to

be in a fully detwinned martensitic state. For a material in such a state, $H^{cur}(\sigma)|_{\sigma \geq \sigma_{align}} = H^{max}$ is the *maximum available transformation strain*. Here the quantity σ_{align} denotes the minimum stress sufficient to fully align the martensitic variants. For sufficiently trained materials, the value of σ_{align} may approach zero. Transformation strain evolution will be further addressed in Sect. 3.3.3.

Other than the value of the maximum transformation strain, it is also important to note the manner in which the strain evolves during loading. Some materials will show a distinct transition from elastic response to transformation and little stress increase during transformation. This is an indication of limited 'hardening' (An example of this will be shown in Sect. 2.5.1). Other SMAs will transition smoothly from elastic to transformation and may show a large increase in stress as the transformation progresses. These materials exhibit more significant hardening. (An example of this will be shown in Sect. 2.5.2). Different material models exist which account for varying kinds of material hardening, and the experimentalist should take note of this behavior. A more detailed discussion of this will be undertaken in Chapter 3.

With each of the aforementioned properties determined, the elastic behavior of each of the two phases is captured. In addition, the evolution of transformation strain is described and the locations of transformation regions in the stress-temperature space are determined. For the models that will be described in Chapter 3, it is required that only the three classes of properties describing these three attributes of SMA behavior be determined. Of course, more complicated models exist that require additional material parameters to account for more general material behavior. Such behaviors include transformation-induced plasticity and the reorientation of martensite. Models incorporating these behaviors will be discussed in Chapter 5 and Chapter 6, respectively.

2.3 Experimental Characterization Process

To experimentally quantify the properties described above for a given SMA material, one could subject a representative specimen to a wide range of uniquely defined thermomechanical loading paths while monitoring the material response. Years of SMA research worldwide have shown that this range can be narrowed to include only a few key tests. The process of characterization described below follows a natural order useful for determining specific material properties as well as for understanding qualitative material behaviors. Furthermore, it allows for an understanding of unstabilized and trained material behavior, an often overlooked distinction in SMA experimentation and application design.

2.3.1 Overview of the General Thermomechanical Characterization Process

In brief, the experimental process proceeds as follows:

- **Experiment 1:** Determination of zero-stress transformation temperatures
- **Experiment 2:** Monotonic loading/monotonic unloading of specimen
  - a) Load at $T < M_f$ to determine martensitic response and zero-stress SME behavior
  - b) Load at $T > A_f$ to determine austenitic response and pseudoelastic behavior
- **Experiment 3:** Determination of SME at non-zero stress level
- **Experiment 4:** Determine effects of cyclic loading, including material response stabilization

The logic behind these steps is straightforward and is based on forming an evolving understanding of the material behavior. Zero-stress transformation temperatures (Experiment 1) are vital to the remainder of the testing process as they allow for experimental system design. Without some knowledge of these temperatures, the proper thermal testing environment cannot be configured.

Monotonic material loading (Experiment 2) is important as a standard test for most materials in determining elastic behavior. It is further important in SMA characterization because such testing above A_f and below M_f provides important information on the key behaviors of pseudoelastic response and stress-free shape memory effect, respectively.

Experiment 3 expands on the SME results of Experiment 2a, testing the capability of the material to provide work output by generating and recovering transformation strain under non-zero stresses.

Finally, the cyclic loading applied during Experiment 4 highlights the change in material response given a particular loading history. After sufficient cycles, the response will often stabilize. This training can significantly modify the material properties and hence requires the repetition of the characterization process (Experiments 1–3).

2.3.2 Illustration of the General Characterization Process

Given the overview, we now demonstrate the general SMA characterization process in more detail. Consider a NiTi wire sample with a diameter of 0.91 mm intended for use in an actuation application. Because the specimen is in wire form, all reported stresses and strains are uniaxial components as obtained in tension. The uniaxial stress is taken as force over a wire cross-sectional area where testing was performed on an MTS 810 system using a 150-pound load cell. This load frame is shown in Fig. 2.10a. An MTS extensometer with a gauge length of one inch was used to record specimen strain levels.

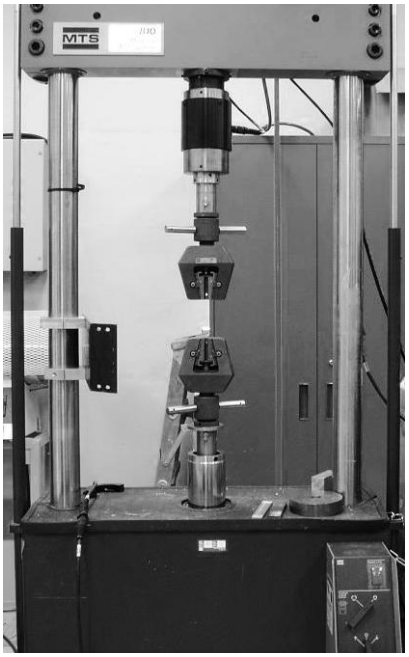

(a) MTS 810 servohydraulic loading frame.

(b) SMA sample loaded into a DSC system.

Fig. 2.10. Experimental equipment used for thermomechanical characterization of shape memory alloys.

Experiment 1: Determination of Zero-Stress Transformation Temperatures

This first experiment is the most fundamental step in the characterization of shape memory alloys. Without knowledge of the stress-free transformation temperatures, it is very difficult to know what phase is present in the alloy at any given stress and temperature state. Recall also that this first experiment is crucial in designing the remainder of the experimental process. To assess these temperatures, a DSC was used (see Sect. 1.8). The small DSC sample is cut from larger bulk material using a low force saw. This method reduces frictional heat and overall material deformation, maximizing the representative integrity of the cut specimen. Note that the use of EDM to cut DSC specimens also leads to accurate DSC results. The specimen is shown being loaded into the DSC machine in Fig. 2.10b, and the test results are shown in Fig. 2.11a. To quantify this heat flow/temperature curve, one may construct lines tangent to the start and finish of each peak and lines tangent to the baseline heat flows. The distinctive intersections of these lines provide one possible measure for the start and finish temperatures of each transformation.

This has been illustrated in Fig. 2.11b, where the transformation temperatures have been noted. It is important to recall, that some materials exhibit the R-phase transformation. For these materials, R-phase transformation indicated in DSC results may be confused with austenitic/martensitic transformations. Given the DSC data alone, it is not always clear if exhibited peaks indicate A→R or A→M, for example. Therefore, the DSC results obtained directly from as-received material should be used as guidelines while zero-stress transformation temperatures derived from other thermomechanical tests are often more practical or applicable in predicting transformation behavior, especially in engineering applications (see the example in Sect. 2.5.1).

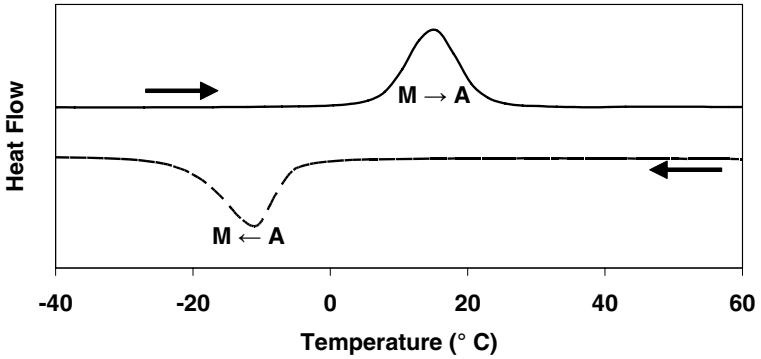

(a) DSC results

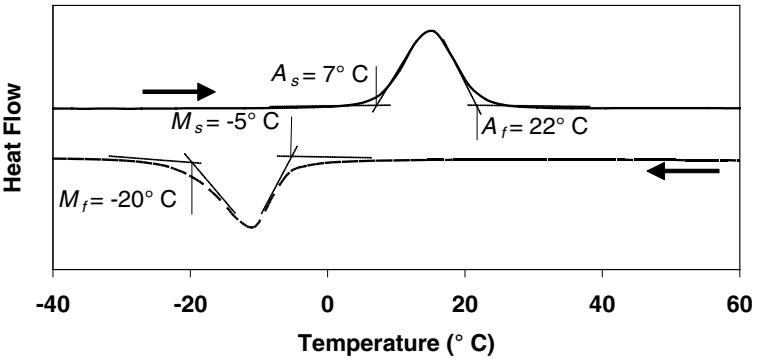

(b) Determination of transformation temperatures using tangent lines

Fig. 2.11. Determination of stress-free transformation temperatures from DSC testing (NiTi, untrained material).

Experiment 2: Monotonic Loading of Specimen

$\mathbf{T < M_f}$:

Monotonic loading below M_f provides information on the elastic properties of twinned (self-accommodated) martensite and determines if the material exhibits crucial shape memory behavior by verifying the capability of the material to exhibit stress-free SME (see Sect. 1.4). Alternatively, additional loading can be applied to failure, to assess the yield and ultimate fracture properties of the particular SMA.

In the current example, data derived from DSC testing is used to determine appropriate testing temperatures. Prior to testing, the sample is first heated above A_f (22°C) to recover any transformation strain and then cooled well below M_f (−20°C) to ensure a fully martensitic material state. This eliminates detwinned martensite which may have formed during inadvertent (and unknown) deformations. The sample is subsequently tested at a temperature below M_f such that martensite is the only stable phase. Testing consists of stressing the material until detwinning completes and to some maximum stress. The maximum stress is not known prior to testing. Rather, it is chosen during the course of testing by noting that detwinning has completed. The sample is then unloaded. The specimen temperature is finally homogeneously increased until it is above A_f, and any strain recovered is monitored.

The results from this test are shown in Fig. 2.12a. Using tangent lines we can approximate the detwinning start and finish stresses as $\sigma_s \approx 140\,\text{MPa}$ and $\sigma_s \approx 170\,\text{MPa}$, respectively. We observe that a significant amount of strain is recovered (6.2%), but some irrecoverable strain remains at the completion of the SME test. This indicates that the material is not responding in a repeatable (stable) manner, and training may be required. Note also that the elastic modulus for martensite is found to be 24 GPa.

$\mathbf{T > A_f}$:

The second monotonic test assesses material behavior at temperatures greater than A_f (i.e., possible pseudoelasticity). Here a loading/unloading cycle is applied to the specimen at $T = 30\,°\text{C}$, and nearly full pseudoelasticity is observed with some residual plastic strain. These results are shown in Fig. 2.12b. The martensitic elastic modulus found here is notably higher than that observed in Fig. 2.12a. This is an important observation and is due to the fact that some remnant austenite may remain at the end of loading. The elastic modulus observed during unloading may then reflect a combination of the moduli of both austenite and martensite. Note that, according to the definitions in ASTM test method F-2516, the *upper plateau stress* or stress at 3% strain during loading is $\simeq 300\,\text{MPa}$. By the same standard, the *lower plateau stress* or stress at 2.5% strain during unloading is $\simeq 100\,\text{MPa}$.

Finally, if device design is a goal, it may be useful to determine the material plastic yield and ultimate failure values. Such a test was not performed on the current specimen, but can be easily accomplished. With respect to the yield

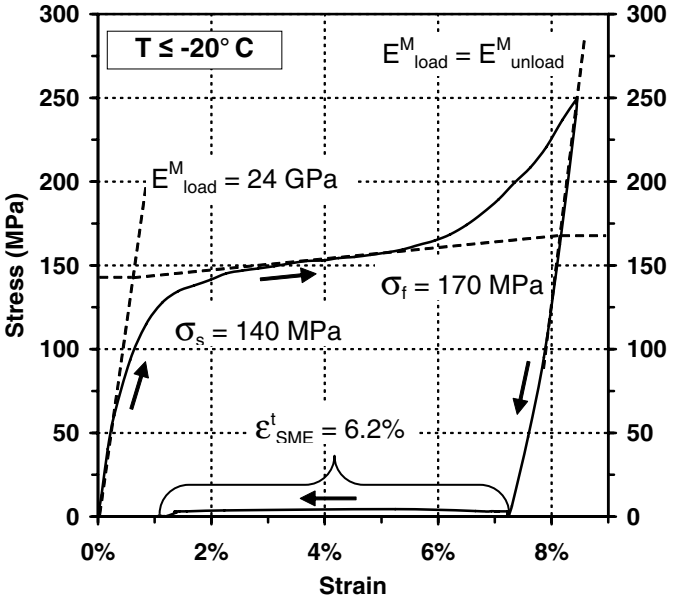

(a) $T < M_f$

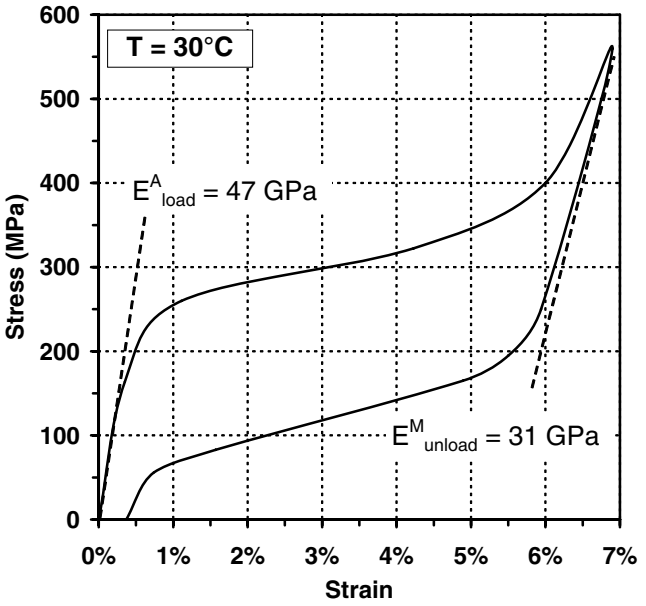

(b) $T > A_f$

Fig. 2.12. Results of monotonic loading/unloading.

and failure properties of martensite, one may employ a used SME specimen to perform these tests. The critical stress for plastic yield is often notably higher than the start and finish stresses for detwinning and should be easily identified. Regarding determination of the austenitic yield limit, note again that such a test must be performed at a temperature sufficiently above A_f to keep the material in the austenitic state (i.e., hot enough to prevent forward transformation into martensite). The phase diagram (estimated or exact) can be used to determine such an appropriate temperature. An additional material property not yet considered, though commonly discussed, is the maximum temperature at which austenite can be transformed to martensite via the application of stress without first plastically yielding. This temperature is often denoted M_d.

Experiment 3: Determination of SME at Non-zero Stress Level

For actuators, it is important to observe not only that the zero-stress shape memory effect is exhibited, but also that the material is able to perform work by providing displacement while under some load. A simple test of this behavior is a constant stress actuation test. In the case of uniaxial loading, this is sometimes referred to as *isobaric* testing. To perform this test for the current example, the material sample is heated well beyond A_f (22 °C) and then stressed to 200 MPa. This load is held constant while the temperature is slowly and homogeneously lowered until forward transformation into martensite is completed. Finally, the temperature is slowly increased until reverse transformation is completed. Throughout this test, the strain is monitored and recorded. The results of this experiment are shown in Fig. 2.13a.

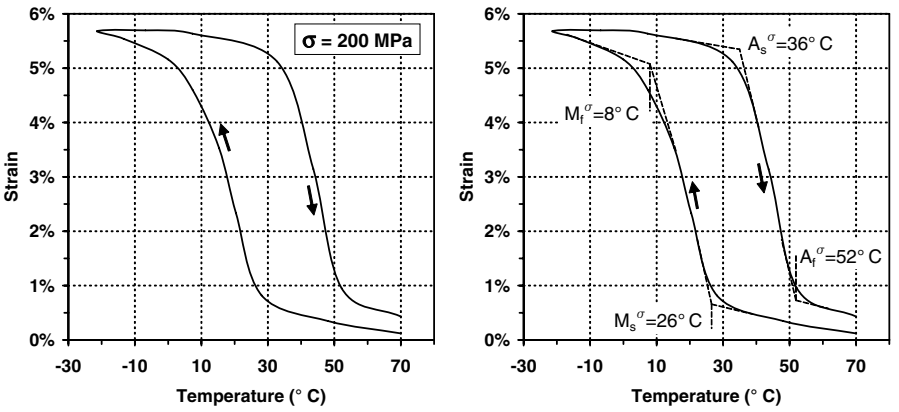

Fig. 2.13. Results of constant stress thermal cycling (first cycle): (a) strain-temperature loading curve, (b) determination of transformation temperatures at stress.

Before continuing with the next experiment in the characterization process, it is appropriate to examine the results observed up to this point. This allows proper planning of additional experiments.

Investigation of Transformation Strain Generation and the Phase Diagram

After completion of the first three experiments, results can be examined and the performance of the material can be assessed. Recalling the three proposed classes of material properties (elastic, transformation criteria, and transformation strain properties), determination of any elastic parameters from the experimental data is often quite straightforward. Properties from the other two classes are addressed at this point.

The ability of the material to generate and then recover transformation strain must be evaluated. It was observed that 6.2% transformation strain was exhibited during stress-free SME testing (Experiment 2a). While this value is important, it is usually more valuable to examine the amount of strain recovered under load. To do so accurately requires not only measuring the total strain generated during transformation, but also considering the contributions of thermal and elastic strains. It is therefore necessary to review the relationship between these quantities.

For the magnitude of strains conventionally experienced by SMAs, the total strain can be additively decomposed into an elastic component, a transformation component, and a thermal component ($\varepsilon = \varepsilon^e + \varepsilon^t + \varepsilon^{th}$). Because the characterization of SMA samples is often 1-D in nature, simple relations can be used to describe the elastic and thermal response at any point in the loading path. In one dimension, the thermal strain may be simply given as $\varepsilon^{th} = \alpha(T - T_0)$ where α denotes the current thermal expansion coefficient. This leads to the following common 1-D elastic relation:

$$\sigma = E[\varepsilon - \varepsilon^t - \alpha(T - T_0)]. \tag{2.3.1}$$

Here the T_0 is assumed to be the reference testing temperature. We can now consider the stress found in the wire when it has been fully transformed into one phase or the other. When the material is purely martensitic, it is fully detwinned such that $\varepsilon^t = H^{cur}(\sigma)$. In this pure martensitic state and at the reference temperature ($(T - T_0) = 0$), this yields the following for the stress in terms of the current total strain:

$$\sigma = E^M[\varepsilon - H^{cur}(\sigma)]. \tag{2.3.2}$$

It is further assumed that when the material is purely austenitic, all transformation strain has been recovered ($\varepsilon^t = 0$). For materials in such an austenitic state, this yields the following for the austenitic stress in terms of the total strain:

$$\sigma = E^A[\varepsilon - \alpha^A (T - T_0)]. \tag{2.3.3}$$

Therefore, given one isobaric test at one given constant stress level (see Fig. 2.13b), one can derive the maximum transformation strain by solving both (2.3.2) and (2.3.3) for the current strain in each of the pure phases and assuming a constant testing stress, σ. This yields:

$$\varepsilon^M = \frac{\sigma}{E^M} + H^{cur}(\sigma), \tag{2.3.4}$$

$$\varepsilon^A = \frac{\sigma}{E^A} + \alpha^A (T - T_0), \tag{2.3.5}$$

where ε^M and ε^A denote strain in a purely martensitic and purely austenitic state, respectively. Observing Fig. 2.8b, the height of a given hysteresis is $\Delta\varepsilon = \varepsilon^M - \varepsilon^A$, which, considering (2.3.4) and (2.3.5), leads to the following relation for the current maximum transformation strain at a given constant stress test level:

$$H^{cur}(\sigma_i) = \Delta\varepsilon + \alpha^A (T - T_0) + \sigma_i \frac{E_M - E_A}{E_M E_A} \tag{2.3.6}$$

Therefore, having determined the elastic moduli of martensite and austenite, and using an appropriate common value for the austenitic coefficient of thermal expansion (10^{-6} [3]), one can derive the maximum transformation strain, $H^{cur}(\sigma_i)$, exhibited under the application of each constant stress σ_i. For the single test performed thus far (Fig. 2.13b) where $\sigma_i = 200\,\text{MPa}$, this is found to be $H^{cur}(200) = 5.1\%$.

It is also important to determine at what stress and temperature states the material can be expected to transform. The transformation criteria are best understood via construction of the phase diagram, which describes the transformation behavior in stress-temperature space. In relation to the progress of the current example, it is now important to have an approximate understanding of the transformation behavior for the purpose of planning a suitable cyclic loading experiment. To construct such an estimation requires two data points per transformation surface, assuming the transformation boundaries are approximately linear. The first set of points can sometimes be estimated via DSC testing (Experiment 1) and indicate at what temperatures the transformations begin and end under zero stress.

The second set of points can be determined from the constant stress actuation cycle (Experiment 3), or from the constant temperature pseudoelastic cycle (Experiment 2b), as applicable. Since the current example involves material intended for actuation, here we determine the discrete transformation temperatures at 200 MPa constant applied stress (Fig. 2.13a). For the purpose of illustration, tangent lines are constructed and their intersections are used to provide discrete values for these non-zero stress transformation temperatures. This is illustrated in Fig. 2.13b. Here M_s^σ and M_f^σ represent the non-zero stress forward transformation start and finish temperatures, respectively. Likewise, A_s^σ and A_f^σ represent the *non-zero stress* reverse transformation

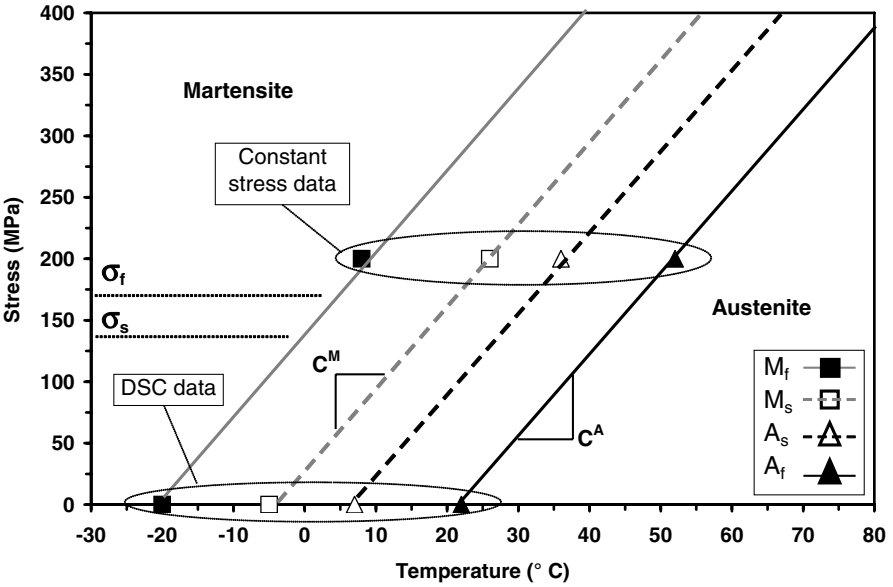

Fig. 2.14. Preliminary phase diagram, as-received material.

start and finish temperatures, respectively. Plotting the stress-free transformation temperatures and the 200 MPa transformation temperatures in the same stress-temperature space, an approximate phase diagram is constructed, as shown in Fig. 2.14. While this approximate phase diagram is insufficient to calibrate a model that accurately captures material behavior at all thermomechanical states, it is useful to estimate at what states the material will be fully austenitic and fully martensitic. It is also useful in planning the training process, as previously mentioned.

Experiment 4: Determination of Cyclic Loading Effects (Training)

To determine the effects of cyclic loading on the thermomechanical response of an SMA, the material is subjected to multiple transformation cycles. In the case of a material intended for use as an actuator, a straightforward method consists of applying many thermal transformation cycles under constant load to the specimen. This is often referred to as *training*. If the goal of cyclic loading is eventual stability of response, training loads (thermal and mechanical) which exceed those expected in the application should be applied (see also Sect. 1.6). For the current example, it will be seen that all further experimentation is performed at stress levels of 200 MPa and below. A constant stress of 200 MPa is therefore chosen for cyclic loading. A total of 80 thermal cycles are applied and the results are shown in Fig. 2.15. Note that while the initial strain response of the material evolves with each cycle, it eventually stabilizes.

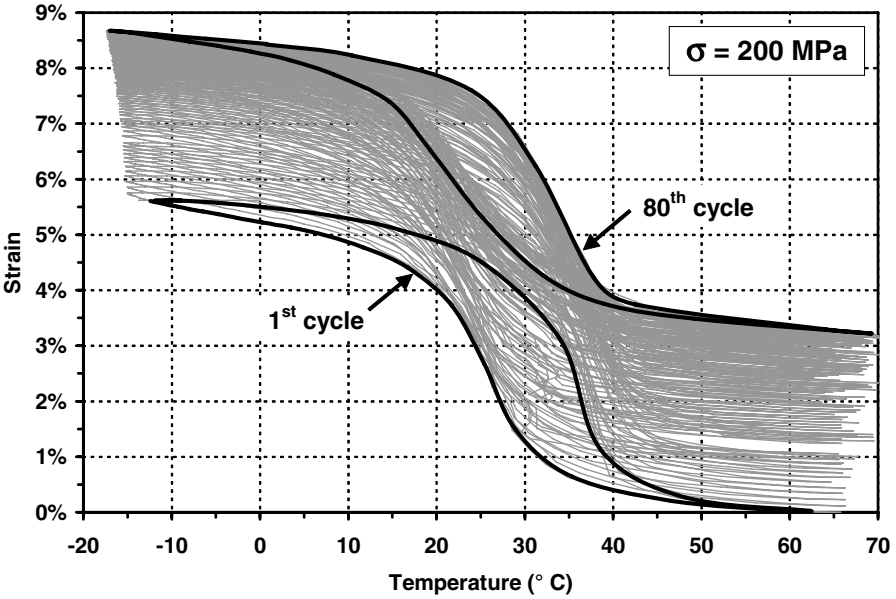

Fig. 2.15. Results from isobaric training at 200 MPa.

As an alternative to constant temperature or constant stress cyclic loading, application-based cycling may be used wherein an SMA specimen is stabilized in the same manner in which it is used (e.g., a smart structure incorporating active SMA elements is repeatedly actuated). The SMA components can then be removed from the application context and tested in the standard manner. Whatever stabilization or training method is used, it is important to remember that the particular choice of loading path used to train a specimen can substantially influence the final material properties and should be carefully chosen.

Evaluation of Stabilized or Trained Material

When a material has been cyclicly loaded and its response has evolved and stabilized, it is necessary to repeat the most important tests of the characterization process to attain the new trained material properties. The results of such repeated testing will be summarized below.

The first interesting and important result involves the effect of training on the DSC test results. During training of polycrystalline SMAs, widespread permanent dislocations are generated at the micro-scale within the material. This results in a heterogeneous microscopic stress state, which, per the behavior characterized by the phase diagram, results in transformation temperatures that vary from locale to locale. Because this occurs throughout the specimen, a distribution of localized transformation temperatures is expected.

This "smoothing" diminishes the usefulness of the DSC results in ascertaining the overall zero-stress transformation temperatures by effectively eliminating the peaks observed during heating and cooling. Therefore, other methods of determining these temperatures are often required after cyclic loading.

Recalling that the intended use of the material in the current example is actuation under some non-zero load, it is clear that a repetition of the stress-free shape recovery testing, or SME testing, is not necessary. Observation of the stabilized constant stress actuation behavior, however, is not only important but necessary for the determination of several material parameters. Determination of the temperatures at which the phase transformations begin and end for different constant stresses allows construction of the final phase diagram.

In addition, by examining the amount of strain generated during each isobaric cycle, one may derive a functional relationship between applied stress and current maximum transformation strain for this stabilized material. To this end, thermal cycles at constant stress are applied to the specimen. Stresses ranged from ~ 2.5 MPa to 200 MPa in ~ 50 MPa increments. The low stress test is important in not only determining the zero-stress transformation temperatures, but also in indicating the presence of transformation strain generation at zero-stress (the so-called "two-way shape memory effect," see Sect. 1.6). The results of these constant stress tests are shown in Fig. 2.16.

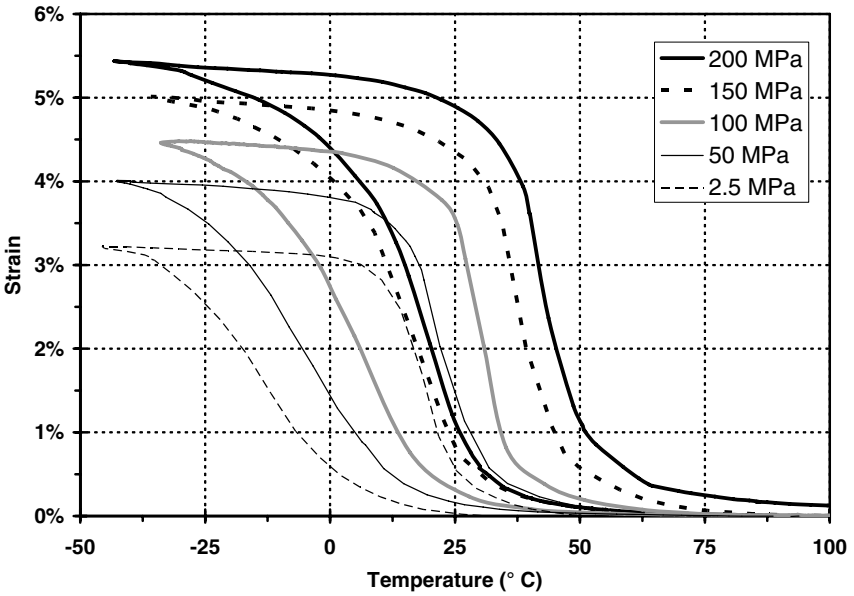

Fig. 2.16. Results of isobaric thermal cycling at various stress levels, trained material.

By examining the constant stress uniaxial test results, the amount of uniaxial transformation strain generated by the material for a given constant stress can be determined. This again requires that 2.3.6 be used to derive the current maximum transformation strain $H^{cur}(\sigma_i)$ exhibited under the application of each constant stress level σ_i. The experimental plot of this relationship is shown in Fig. 2.17. The dashed fitted curve represents the proposed functional form of $H^{cur}(\sigma)$ and highlights the tendency of the current maximum transformation strain to saturate with increasing stress.

Finally, the phase diagram for the stabilized material is derived. To construct the phase diagram (i.e., to determine the transformation temperatures at various constant stress levels), tangent lines are again used as shown in Fig. 2.18. Here the transformation temperatures are investigated for the material under an applied stress of 150 MPa. The experimental phase diagram is derived from a whole series of such tests and is shown in Fig. 2.19. Simple linear regressions are used to schematically represent each of the continuous transformation surfaces. One key change from the untrained, estimated phase diagram is the obvious broadening of the transformation regions (see Fig. 2.14). The mechanisms behind this behavior are the same as those previously discussed concerning the reduced usefulness of the DSC results. However, extrapolation of the transformation surfaces supersedes the DSC in providing an accurate indication of the zero-stress transformation temperatures.

The derived material properties for the experimental study summarized in this example are given in Table 2.1. Most properties were determined for the stabilized material, with the exception of elastic moduli.

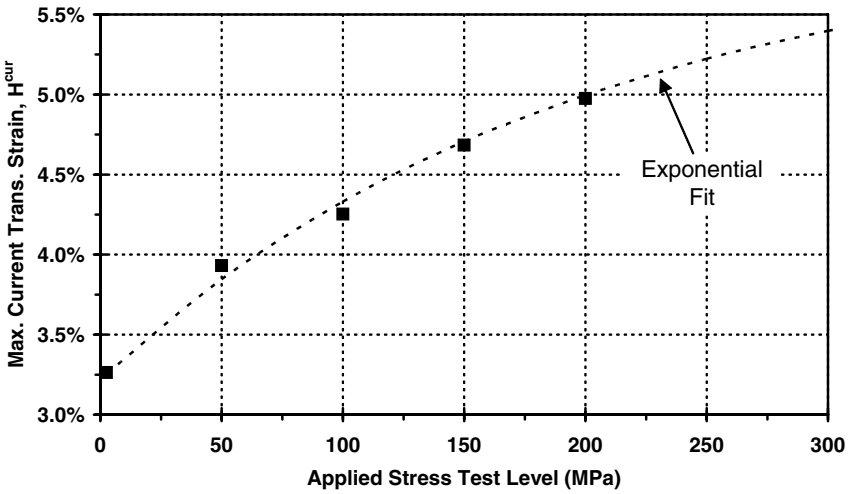

Fig. 2.17. Determination of exhibited maximum transformation strain as a function of applied constant stress, trained material.

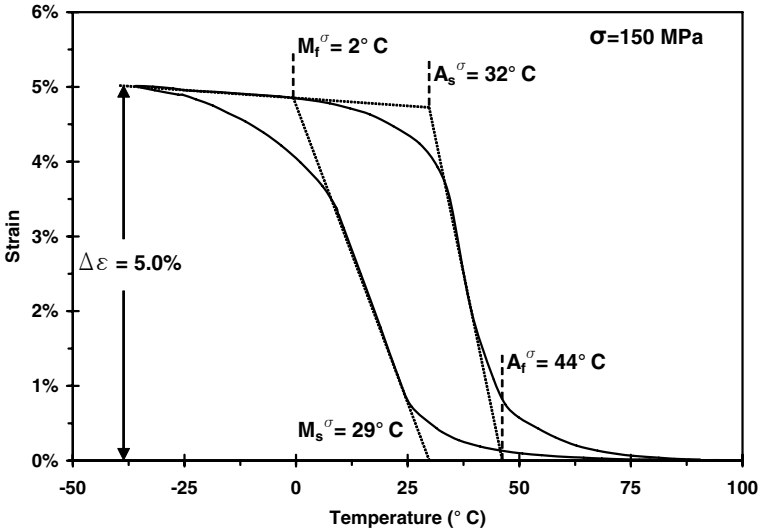

Fig. 2.18. Determination of transformation temperatures using tangent lines at a constant stress of 150 MPa, trained material.

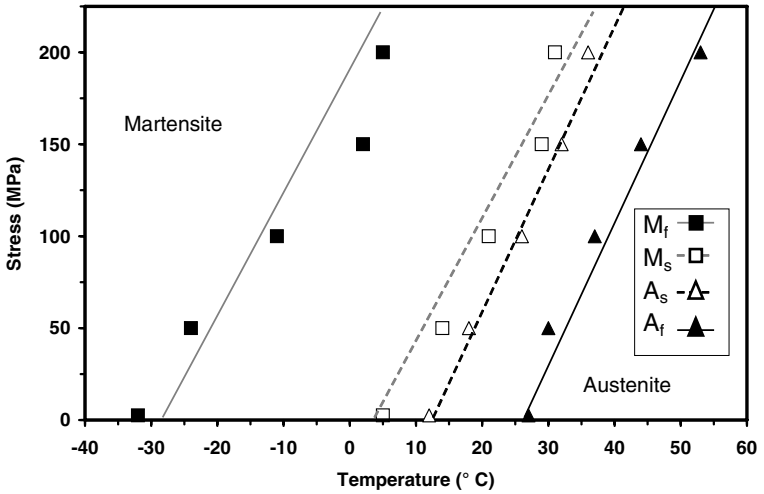

Fig. 2.19. Experimentally derived phase diagram, trained material.

This concludes the general characterization process for a particular example of SMA material. While interesting material behaviors such as fatigue, plastic hardening, transformation-induced plasticity, or others could also be studied, these will not be covered at this time. The intent of the above example was an illustrated overview of the most common experiments. However, while the characterization process for SMA specimens is conceptually straightforward,

Table 2.1. Experimentally derived material parameters; trained material.

Material Parameter	Value
E^A	47 GPa
E^M	24 GPa
σ_s	140 MPa
σ_f	170 MPa
M_s	3 °C
M_f	−29 °C
A_s	12 °C
A_f	26 °C
C^A	8.3 MPa/ °C
C^M	6.7 MPa/ °C
$H^{cur}(\sigma)$	$= H^{cur}(0) + (H^{max} - H^{cur}(0))[1 - \exp(-k_H\sigma/E^A)]$
	$= 0.032 + (0.06 - 0.032)[1 - \exp(-235\sigma/E^A)]$

there are many unique challenges that the SMA experimentalist must address. Such considerations will now be discussed.

2.4 Experimental Considerations Unique to SMA Thermomechanical Characterization

In the previous section, a description of a characterization procedure for SMAs was given and instructions for the completion of each experimental step were provided. However, the unique properties of SMAs are eventually manifested as a set of important experimental details and challenges that must also be discussed. These topics include consideration of loading rates, material statistical variation, material history, etc., and will be described with others in more detail below.

2.4.1 Influence of Total Material History on Shape Memory Behavior

As with other metals, the constitutive properties of shape memory alloys are strongly dependent on several factors, including the exact alloy composition, the particular heat treatments previously applied, prior history, and cold-working. However, because SMAs undergo important microstructural changes not attainable in other metallic systems, the material sensitivity to these and other historical occurrences can be much higher in thermomechanical response. The designer must be aware of these effects during the material selection phase, and it is important that the experimentalist keeps these details in mind to ensure accurate and representative testing.

The most influential characteristic of a material specimen is its alloy composition. As previously reviewed (see Sec. 1.9), several alloy systems are

known to exhibit shape memory behavior (NiTi, NiTiCu, NiMnGa, etc.), and each has significantly different properties. It is reasonable that a change in elemental constituents will cause a change in exhibited material behavior. However, SMAs are also highly sensitive to the atomic balance when considering even just one alloy system (i.e., NiTi). A very small change in the balance between nickel and titanium will noticeably affect properties, especially with respect to the transformation temperatures. Furthermore, two material specimens of nominally identical composition will often behave dissimilarly. In this way, the sensitivity of shape memory alloys to composition surpasses that of aluminum, iron and other more conventional metals. For SMAs, one cannot often define a required set of material properties and then accurately choose a material composition that will provide them (though it is possible to estimate an appropriate composition).

It has also been shown that the exact thermomechanical response of an SMA is highly sensitive to heat treatments. This is because imposed thermal manipulations, such as high temperature soaks and rapid quenches, greatly affect a metal at the microscopic scale. Internal stresses can be generated or relaxed, and precipitates can be formed or dissolved. As with other metals, alterations in the elastic, plastic and ultimate failure properties will occur. In addition, transformation temperatures will shift, and even the ability of the alloy to exhibit some effects will improve or degrade (i.e., pseudoelasticity). For example, pseudoelasticity is rarely observed in some NiTi systems that have been fully annealed and is only possible if sufficient precipitates are formed via aging or other such treatments [25].

Like heat treatments, cold-working and hot-working performed during material processing can significantly alter material behavior. Examples of such working important to the SMA experimentalist include the drawing of raw material into wires or the rolling of the material into plates. Such permanent deformations can induce significant internal stresses while also altering the configuration of the microstructure. The density of dislocations increases and the configuration of precipitates formed during initial fabrication and heat treatment can be altered (see Sect. 1.9.1).

Perhaps a more fundamental effect of such processes is the alteration of the grain structure. Grains are often refined, but can also be notably reoriented, inducing material anisotropy and texturing effects. Such material alterations continue to occur during specimen preparation and testing. The thermomechanical conditions imposed during material specimen training are especially influential on the final properties and should be chosen carefully. As with heat treatments, microstructural changes incurred during working will alter both the conventional and especially the shape memory properties of SMAs.

These and other considerations lead to an important conclusion, especially when design of some application is the goal: to accurately characterize a material, one must ensure that the configuration and history of the SMA test specimen matches that of the SMA component used to the intended application component.

2.4.2 Comparison of Test Specimen to Intended Application Component

For designers and analysts, the end goal of material characterization is often the eventual ability to predict the response of some application, and carefully planned and executed characterization is required for such correct model calibration. The material composition and loads chosen for characterization must be highly representative of those found in the final application system. Between the material intended for use in an application and the complimentary material used for characterization, a one-to-one correspondence is required for the following attributes, several of which have been previously discussed:

1. The exact alloy composition.
2. The methodology of fabrication of the alloy component, including hot/cold working and heat treatments.
3. The loading history of the material prior to use (i.e., thermomechanically stabilized or untrained).
4. The stress state applied (e.g., axial, shear, or multicomponent).
5. The thermomechanical loading path applied, especially in relation to the phase diagram.

The first two of these items are common to the characterization and application of all classes of materials. It is necessary to characterize the same material that is to be used in the application. This includes materials with the same composition, same microstructural texture (as a result of any cold-working), and same heat treatment history.

The third of these items also pertains to other material classes in some degree. However, it is especially important for materials such as SMAs that undergo large deformations and may, over some number of cycles, accumulate significant irrecoverable plastic strain. The generation of this strain results from significant changes in the microstructure of the material, indicating that other material properties may have been altered. As an example, SMA specimens that have been cycled many times and have generated significant plastic strain will often exhibit less maximum transformation strain than was shown before these cycles were applied. It is also common for the transformation regions to broaden (i.e., the difference between M_s and M_f increases). Each of these effects were observed in Section 2.3.1. In the case of a multi-use actuator application, a stabilized material specimen should be characterized. If an application is to be used very few times, or only once, as in the case of some release mechanisms (see Sect. 1.10), then as-received, non-stabilized specimens of identical composition should be characterized. Experimentation itself necessarily imposes loading cycles and that material property evolution is strongest during the first repetitions of loading. Thus, if as-received (non-stabilized) behavior is required, used specimens should be replaced often with new, untested specimens.

It is also important to consider the applied stress state used to derive the material constants. The similarity between the stress state applied during characterization and that experienced by a component in an application has been shown to affect the material parameter calibration accuracy. Specifically, this concerns the distinction between extension vs. shear. Tension/compression asymmetry is also common, and this stress state should be considered as well. If an SMA component undergoes loading consisting mainly of axial tension and/or compression (i.e., wire or rod applications), uniaxial testing should be used. For shear-based applications (i.e., torque tubes, etc.), characterization in shear will often lead to more accurate modeling. In this way G^A and G^M, the shear moduli for austenite and martensite, respectively, may be directly and accurately determined. Furthermore, material for use in tensile applications should be characterized in tension, and similarly for compression.

Finally, let's consider the thermomechanical (stress or temperature) loading path applied to the SMA component of interest during common use. Because the micromechanical consequences of repeated constant stress loading may differ from those of repeated isothermal loading, material properties measured in each of these two ways have been shown to differ significantly. If a design requires an SMA component to undergo nominally isothermal loading (i.e., vibration isolation and other pseudoelastic applications), then isothermal material characterization will be the most accurate. The same requirement applies for components undergoing thermal actuation cycles.

2.4.3 Importance of Mechanical and Thermal Loading Rates

Recall that the forward transformation into martensite is exothermic while the reverse transformation into austenite is endothermic. This introduction of the latent heat phenomenon and resulting possible temperature changes during the characterization process imposes additional constraints on the loading rates applied to SMA specimens. The challenge is particularly applicable to pseudoelastic testing. Such experiments are often performed at constant temperature to simplify interpretation of the transformation behavior. During loading, however, thermal energy can be added to the specimen if the heat generated during the exothermic forward transformation is not dissipated. If loading is performed slow enough, convective and conductive processes will remove this additional heat without noticeably raising the specimen temperature. If loading or unloading progresses too rapidly, the temperature of the specimen will rise during loading and fall during unloading, violating any isothermal assumptions.

Several studies have been performed to assess the influence of loading rates on material response. Many of these address pseudoelastic loading [12, 28, 29] and have found the thermal effects present during this exothermic/endothermic cycle to be significant, especially at higher rates. Throughout the various research efforts in the area of shape memory alloys, many

displacement and thermal loading rates have been suggested. For isothermal loading at any temperature, rates should not exceed $\sim$ 0.01-0.05% strain/sec [12, 18]. This helps to ensure quasi-static testing. Others have also explored the martensitic reorientation (detwinning) rate dependency in various stress configurations and in various alloys [24, 30], and have shown that the detwinning process is generally independent of the strain rate.

Finally, dynamic impact testing has also been performed in several studies [31, 32] and phenomenological model predications and experimental results have been compared while others [33] have investigated martensitic transformation mechanisms under these dynamic loading conditions.

The use of reasonable strain rates is straightforward in strain-driven or deformation-driven experimentation, but not all thermomechanical experiments on metals are performed using prescribed strain or displacement inputs. Most testing systems also provide the option to use force control, which may present advantages in some situations. For example, using force control during pseudoelastic unloading allows the experimentalist to set an exact ending force value, such as 0 MPa or 7 MPa for ASTM standard testing [18]. However, for SMAs exhibiting "flat" pseudoelastic loading/unloading plateaus, force control can lead to problems. A constant force rate that is suitable during the elastic portion of loading quickly leads to an unacceptably high strain rate during stress-induced transformation as the testing system seeks to provide the same constant force rate. An example of this is shown in Fig. 2.20.

Here the main result involves a specimen undergoing two pseudoelastic loading cycles at an ambient temperature of 37 °C (nominal). For the first test, a strain rate of $0.05\%/s$ was applied during both loading and unloading. For the second test, a strain rate of $0.05\%/s$ was applied during loading, but a 0.08 N/s force rate was applied during unloading. In Fig. 2.20a the forward loading (forward transformation) paths for both tests are nearly identical while the unloading (reverse transformation) curves are not. During unloading, the use of force control in the second test caused high strain rates as the material response reached the lower plateau stress. This in turn caused a reduction in specimen temperature from 37 °C to 35 °C as seen in Fig. 2.20b. This temperature change causes the unloading curve to follow a different isothermal load path (i.e., the result for a test temperature of 35 °C) at the end of reverse transformation.

Whatever the deformation rate imposed, the measurement of deformations and strains requires careful attention. In some specimen configurations, the stress-induced strains that result from martensitic transformation or reorientation can initiate at discrete locations and then propagate in a wave-like manner along the length of the test section [34]. For this reason, devices such as strain gauges with short gauge lengths are not particularly effective at measuring the macroscopic strain. Instead, they have been shown to indicate "jumps" in strain as transformation or reorientation is initiated in the local region where the strain gauge is attached [12]. Extensometers, which generally have larger gauge lengths, have been more effective for measuring

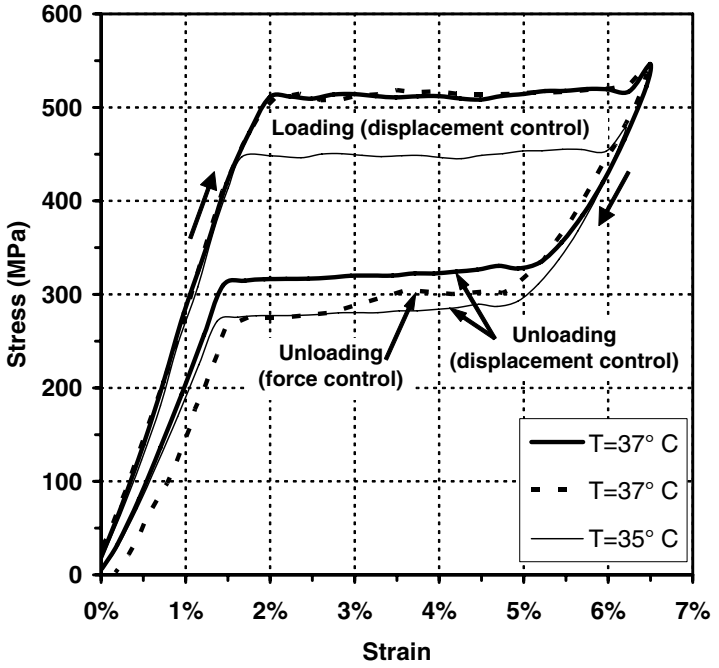

(a)

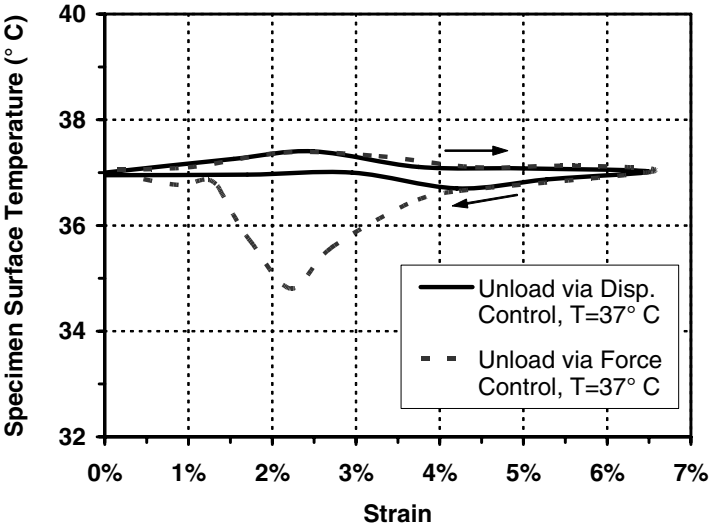

(b)

Fig. 2.20. Comparison of unloading control methods for pseudoelastic testing: (a) stress-strain response, (b) specimen surface temperature response.

phenomenological response. Furthermore, the initiation of phase transformation or martensite reorientation often occurs near the grips and this can lead to inconsistencies when comparing strain measurement acquired over the entire length of a specimen (i.e., via crosshead displacement) with those acquired in a region of homogeneous stress (i.e., via extensometry).

It is also important to impose reasonable heating and cooling rates when prescribed thermal variations are imposed. For specimens such as wires, direct resistive Joule heating is common, while in other cases load frame-mounted furnaces are required. To cool the specimen, conventional liquid baths such as chilled water [12] or laboratory coolant [35] have been used, especially for the testing of wires. For temperatures substantially below room temperature, cooling can be provided by the use of liquid nitrogen [7]. While the mechanical strain rates described above for isothermal testing are generally agreed upon, appropriate heating and cooling rates are often more dependent on the experimental system employed. Such rates must be carefully considered and should be adjusted as necessary to ensure slow, homogenous heating/cooling of the material sample test section.

2.4.4 Stochastic Variation in Material Response

One must also consider stochastic or statistical variation across different material samples. The thermomechanical behavior from specimen to specimen and test to test will often deviate noticeably from some nominal response. To correctly perform material characterization, several material samples for each thermomechanical loading path are often required. Statistical variation may be minimized by ensuring that samples are prepared from homogeneous bulk material in a repeatable manner. However, despite such efforts, some variation will occur and this must be accounted for during subsequent interpretation of results, calibration of any models, design, and analysis. An example is provided in the ASTM standard for DSC testing (ASTM F-2004), where the repeatability across multiple samples is briefly discussed [16]. This issue will be further exemplified in Example 2 in the following section.

2.5 Examples of SMA Characterization

Having expanded on various details of SMA characterization, this section highlights how different considerations affect both the planning and execution of material characterization. Here, three examples are presented. The first demonstrates SMA wire specimens for use in a pseudoelastic application. The second addresses pseudoelastic testing once more, though the focus is the stochastic variation observed when several specimens are taken from the same source material. Finally, the third example illustrates the derivation of material parameters used to model an actuation application in which the material used is not the common equiatomic NiTi.

2.5.1 Example 1. Characterization of NiTi Wire Intended for Pseudoelastic Application

For the first example of characterization, consider conventional, commercially available NiTi wire, intended for use in an application requiring wire components and stabilized material response. Because the material raw form (wire) is the same as the form needed for the application, specimen preparation is minimal. The application is used for vibration isolation research and thus requires an SMA that displays pseudoelasticity at room temperature. The as-received spooled wire fulfills this requirement.

As outlined above, the first step in the characterization process is the estimation of the zero-stress transformation temperatures for the as-received material. DSC testing was again used, and the results from this test are shown in Fig. 2.21.

The next pertinent step is monotonic mechanical testing of the material. However, in this example the response of the material below M_f was of little interest, and the shape memory behavior of the material was not assessed. To plan the pseudoelastic testing process, the experimentalist noted that the A_f temperature estimated from the DSC was $\approx 20\,^{\circ}\mathrm{C}$, below room temperature. This indicates that the first loading path can be applied at room temperature. However, to ensure that the wire temperature remains constant, a heating and cooling system was installed to negate the effects of self-heating and self-cooling during the exothermic and endothermic transformations (2.4.3). This precaution was indeed a necessity as the applied strain rate of 0.13% strain/sec used in this case exceeded the recommendations of Sect. 2.4.3.

The final decision left to the experimentalist was the maximum stress level applied. It is common to decide on this value during testing, while monitoring the stress *in situ*. The maximum stress should clearly exceed the end of forward transformation, but should not be so high as to initiate permanent plastic yielding.

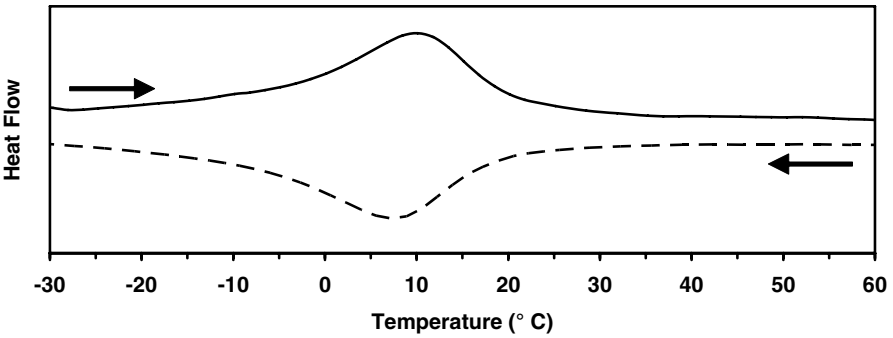

Fig. 2.21. Estimation of zero-stress transformation temperature using a DSC; Example 1, as-received material.

After an initial isothermal loading cycle was performed, the experimentalist noted acceptable results. Thus cyclic loading was commenced to stabilize the material. Recall also that the intended application will be used at room temperature. This further supports 21 °C as an optimal training temperature. Training was performed by applying 15 sequential loading/unloading cycles with a maximum stress of 700 MPa. The results for all applied cycles are shown in Fig. 2.22, with the final cycle highlighted. No significant plastic strain is generated at the end of this last cycle. This material exhibits relatively low hardening with very distinct transitions from elastic to transformation.

With the material satisfactorily stabilized, the experimentalist repeats the characterization process with the goal of deriving final material parameters. Continuing, isothermal loading is applied to the trained wire specimens at different constant temperatures (25, 35, 45, and 55 °C). By noting where transformations begin and end, a new, detailed, phase diagram can be constructed. By measuring different shape parameters found in each pseudoelastic curve, elastic properties and the maximum transformation strain can be derived as shown below. Figure 2.23 shows the pseudoelastic curves for all four constant temperatures at which the SMA wire was tested. To provide a more detailed illustration of material parameter derivation, refer to Fig. 2.24, which shows the material response during testing at 25 °C. Here E^A and E^M are measured in a straightforward manner. Although there appear to be two possible martensitic elastic slopes in this figure (loading and unloading), the slope during loading is influenced by very minor continuing transformation in some

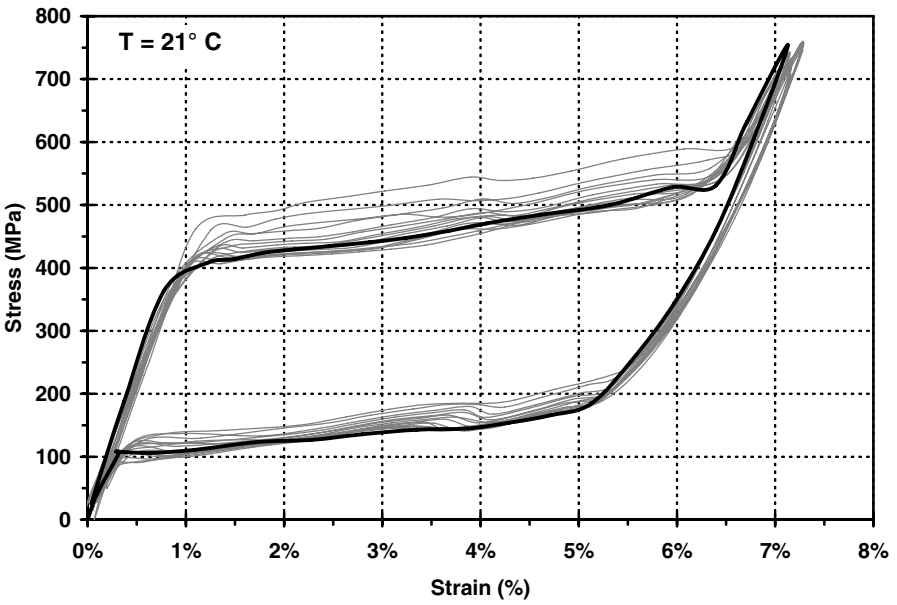

Fig. 2.22. Pseudoelastic stabilization of material at $T = 21$ °C. 15 cycles applied, last cycle darkened.

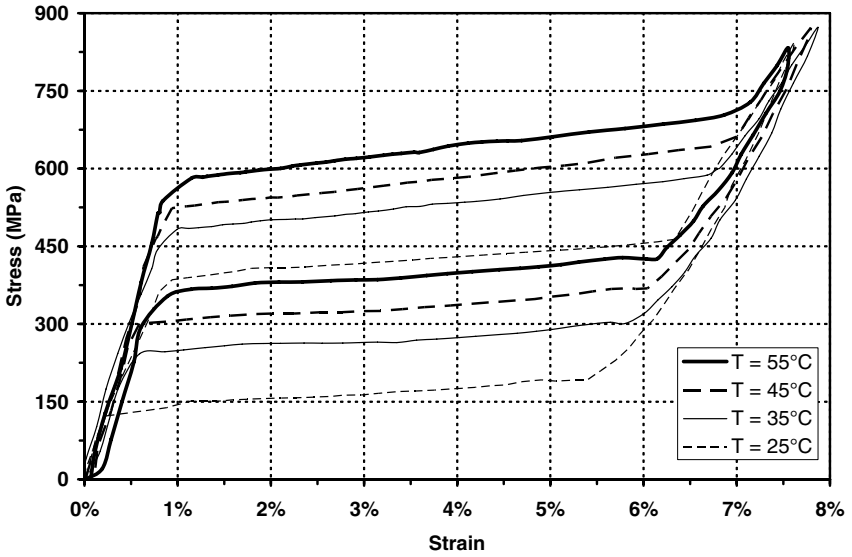

Fig. 2.23. Pseudoelastic loading/unloading results for various testing temperatures.

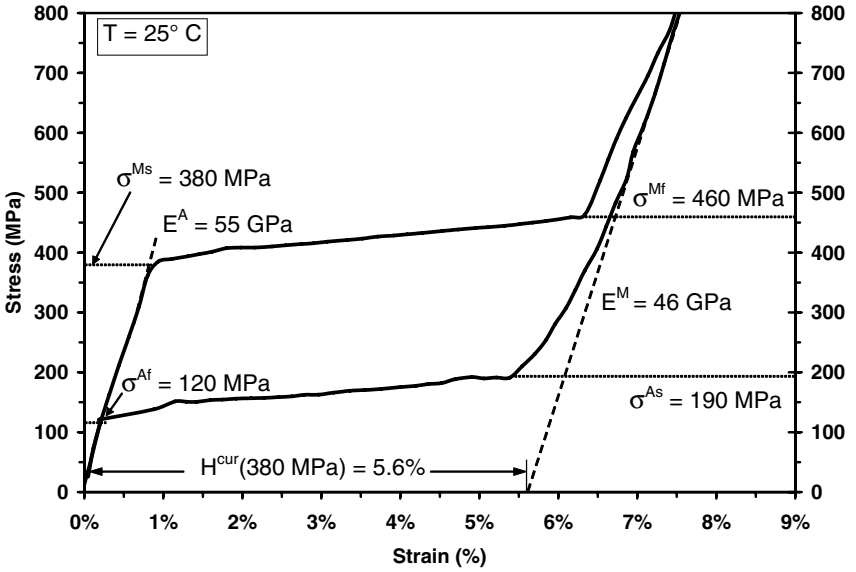

Fig. 2.24. Pseudoelastic loading/unloading results and derivation of parameters for various testing temperatures of 25 °C.

parts of the specimen. The slope during unloading is therefore more representative of truly elastic response. Since the analysis and testing are for 1-D case, ν^A and ν^M are not needed.

The next step is to determine the critical stresses for initiation and completion of phase transformation. At a known constant temperature, these stresses are denoted as σ^{Ms} and σ^{Mf} for martensite and σ^{As} and σ^{Af} for austenite. The values for these stresses at a test temperature of 25 °C are shown in Fig. 2.24. By examining the four isothermal pseudoelastic tests performed (Fig. 2.23), one can determine the stresses for the initiation and completion of both transformations at four distinct temperatures. Construction of the phase diagram proceeds using this experimental data, and results for the current case are shown in Fig. 2.25. The various material parameters found during this experimental study are summarized in Table 2.2.

In addition to the determination of the final phase diagram, the maximum transformation strain, H^{cur}, was also derived. This value is found by considering again (2.3.2) and solving it for H^{cur}. This yields the following relation:

$$H^{cur} = \varepsilon - \frac{\sigma}{E^M} \tag{2.5.7}$$

where the stress used in this relation to determine the current maximum transformation strain is σ^{Ms}. Therefore, given a set of pseudoelastic test results such as those shown in Fig. 2.24, and considering an imagined martensitic stress of zero, it can be inferred that the maximum transformation strain, H^{cur}, is equivalent to the amount of strain indicated when the martensitic elastic stress response is extrapolated to the zero-stress axis. This has been shown in Fig. 2.24.

One key feature of these results is the incompatibility between the phase diagram (Fig. 2.25) and the DSC results (Fig. 2.21). The DSC was performed on the as-received specimen without any preparatory heat treatment (see ASTM F-2004 [16]). The results indicate transformation temperatures at zero-stress that do not agree with those derived from the phase diagram via extrapolation. As mentioned previously, this apparent contradiction is not uncommon in materials exhibiting R-phase transformations (e.g., nickel-rich NiTi alloys).

Table 2.2. Experimentally derived material parameters; Example 1, trained material.

Material Parameter	Value
E^A	55 GPa
E^M	46 GPa
M_s	−28 °C
M_f	−43 °C
A_s	−3 °C
A_f	7 °C
$C^A = C^M$	7.4 MPa/ °C
$H^{cur}(\sigma) = H^{max}$	0.056

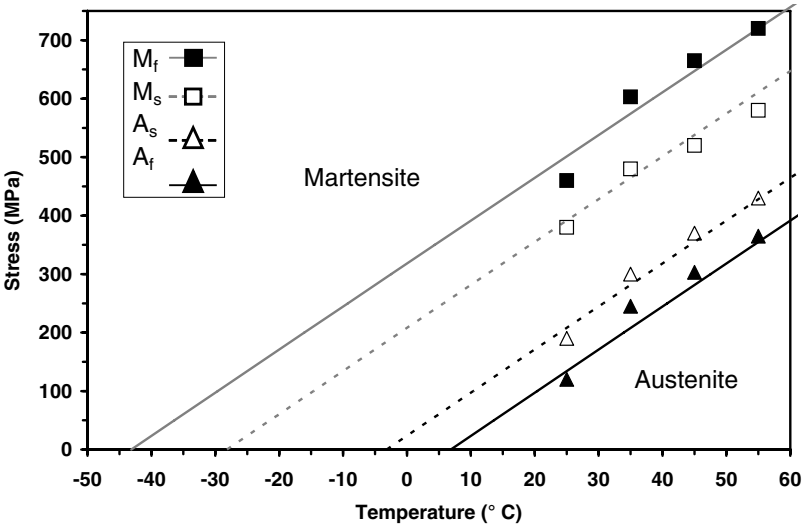

Fig. 2.25. Experimental estimation of phase diagram using pseudoelastic experiments; Example 1, trained material.

2.5.2 Example 2. Characterization of NiTi Wire for Determination of Stochastic Variation

This example is intended to illustrate only the effects of stochastic variation across samples (see Sect. 2.3) where the effect of interest was pseudoelasticity. Four NiTi (50.3 Ni, at.%) wire samples with a diameter of 2.16 mm were used, each taken from the same original roll and prepared (i.e., heat treated) in a consistent manner.

The zero-stress transformation temperatures of the material were first determined via DSC testing. The heat flow curves for the heating portion of the tests for each of the first three wires are shown in Fig. 2.26. Note the slight variation in the results for wire specimens from the same source and prepared in the same manner.

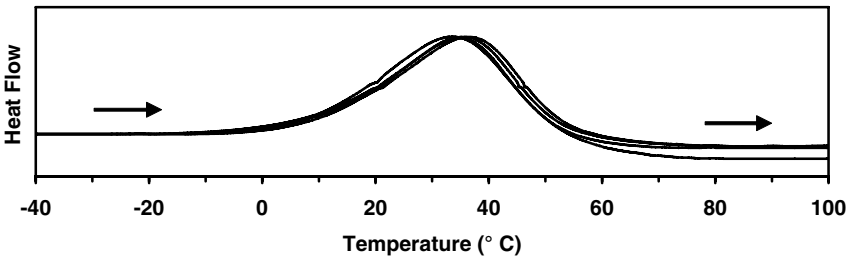

Fig. 2.26. DSC results (heating cycle) showing slight variation across four wires; Example 2, as-received material.

Based on the results of the DSC, it was determined that 80°C was an appropriate constant temperature at which to test the pseudoelastic characteristics of the wire samples. The first of the four specimens was loaded to ≈ 800 MPa and then unloaded. Such a load was repeated 20 times to stabilize the material. The results of this pseudoelastic testing can be seen below in Fig. 2.27. Note the substantial reduction in the pseudoelastic hysteresis caused by repeated application and removal of the load.

To assess the stochastic variation across multiple samples, this same loading scheme was applied to each of the remaining three wire specimens. Stress/strain results for the first cycle and the last cycle were then plotted and compared. These results can be seen in Fig. 2.28. Here it is observed that the statistical variation in the response of the specimens is not negligible, and is more noticeable than the variation in their DSC results (Fig. 2.26). While the qualitative behavior exhibited by the first cycle and the stabilized 20^{th} cycle is similar for all samples, there is a marked variation in each response. Perhaps most notable is the inconsistency in the material hardening observed in each wire during the final loading cycle. Such a result reiterates the need for designers and analysts to always account for some statistical error when deriving model parameters from experimental data. The material properties averaged across the four samples are given in Table 2.3. Because tests were not performed at varying temperatures, no accurate phase diagram parameters were derived.

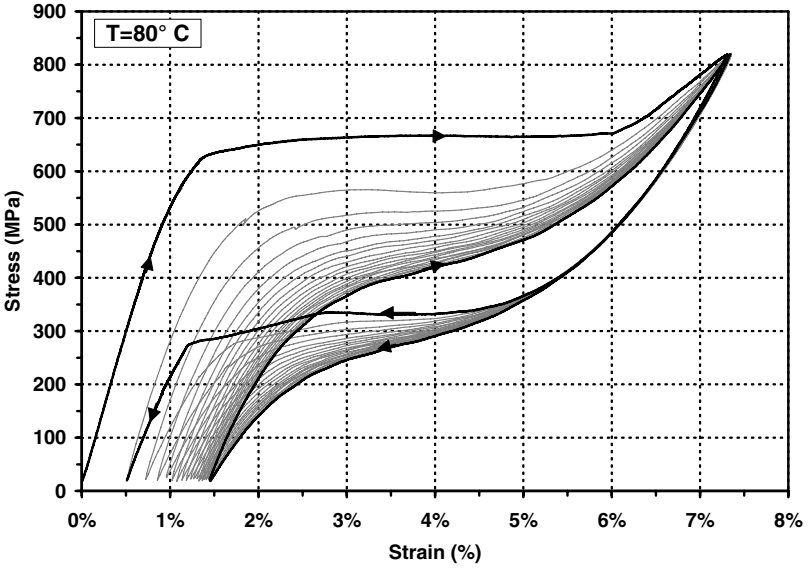

Fig. 2.27. Results of repeated pseudoelastic testing of large diameter NiTi wires; Example 2, training of material.

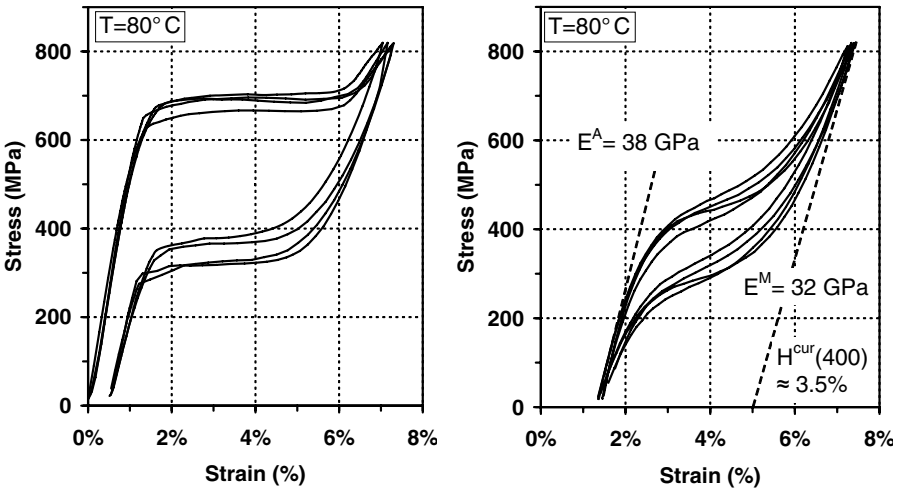

(a) Four wires, 1^{st} cycle (as-received) (b) Four wires, 20^{th} cycle

Fig. 2.28. Results of pseudoelastic testing of multiple large diameter wire specimens from same bulk NiTi material; Example 2, as-received and trained material.

Table 2.3. Experimentally derived material parameters; Example 2, trained material.

Material Parameter	Value
E^A	38 GPa
E^M	32 GPa
$H^{cur}(\sigma) = H^{max}$	0.035

2.5.3 Example 3. Characterization of Ni60Ti40 (wt%) Plate Intended for Actuation Application

This example pertains to the characterization of a NiTi alloy intended for use in an actuation application. The material received for testing was in the form of plates 267 mm long, 38 mm wide, and 1.8 mm thick. The SMA components as utilized in the application were in a beam configuration, providing a bending moment to the aerostructure on which they were mounted. This implies that the most prominent stresses within the SMA component would be axial and would vary throughout the component. This experimental study provided an opportunity to showcase how simple 1-D characterization could be used to predict the performance of a 3-D SMA component experiencing complex internal stresses. Thus, careful and accurate model calibration was required. Also, the application is intended to be used repeatedly. Stable material response is then required.

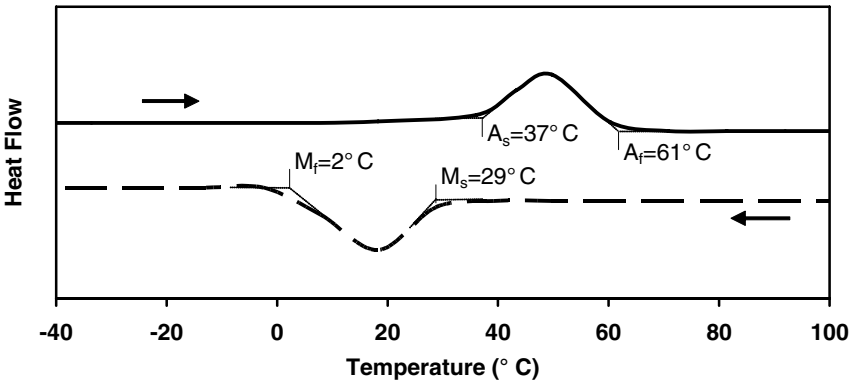

Fig. 2.29. Determination of zero-stress transformation temperatures using a DSC; Example 3, as-received material.

Here, as before, the first step was to determine the zero-stress transformation temperatures via DSC testing. For this purpose, small portions ($\sim 20\,\text{mg}$) were cut from the received plate with a low force saw. The results of DSC testing are are shown in Fig. 2.29.

The next step was to subject the material to monotonic loading. The first test was performed at $T < M_f$, and the results are given in Fig. 2.30a. As is often the case, the maximum stress was not known beforehand but was chosen during testing such that the majority of detwinning was completed, yet obvious plastic yielding did not begin to occur. For some SMAs, such as the material in this example, the detwinning start stress may be clearly observed during testing while the detwinning finish stress may be less clear (or completely obscured) due to significant material hardening and plastic strain generation. In this case, an accurate determination of the detwinning start stress is useful, and $\sigma_s \approx 140\,\text{MPa}$ was calculated using tangent lines. Upon unloading, the specimen was heated to above A_f, and the recoverable transformation strain was recorded. This material does not exhibit recoverable strains of the same magnitude as those seen in equiatomic NiTi materials (Sect. 1.9.1).

Following monotonic testing below M_f, such loading was repeated at $T > A_f$. A moderate load was applied and the elastic modulus of austenite was determined. Because of the intended use of the material in an actuation application, pseudoelasticity was not of direct interest and the specimen was not loaded sufficiently to induce this effect. The results for $T > A_f$ are shown in Fig. 2.30b.

The material specimen was then subjected to isobaric thermal cycles. Based on knowledge of the stresses to be expected in the final application, a moderate constant loading level of 150 MPa was chosen. The results of this test are shown in Fig. 2.31. Note the significant amount of plastic strain remaining at the end of the test, this indicates a certain need for material

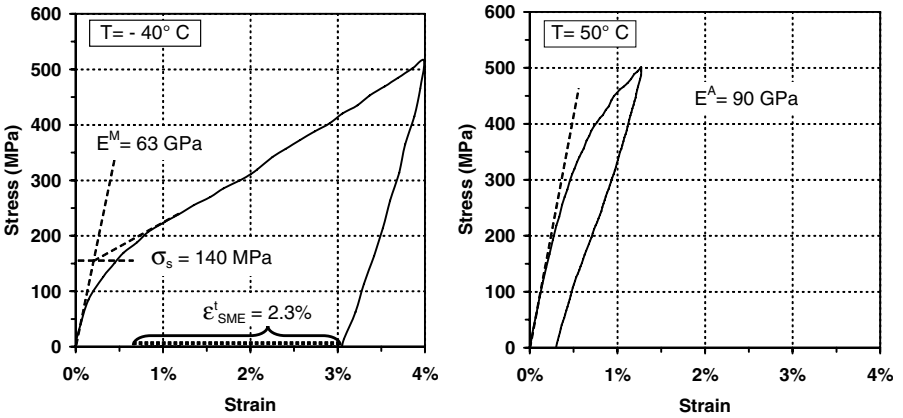

(a) $T < M_f$ and SME recovery (b) $T > A_f$

Fig. 2.30. Monotonic loading of Ni60Ti40 (wt. %) material in martensite and austenite; Example 3, as-received material.

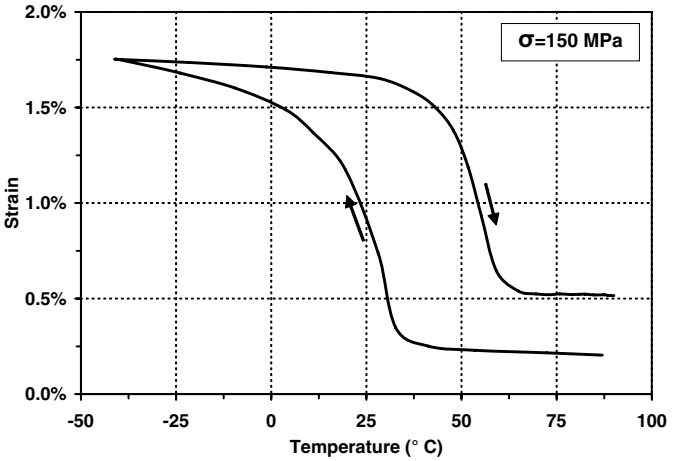

Fig. 2.31. Results of first isobaric test at 150MPa; Example 3, as-received material.

training. Plotting both the zero-stress transformation temperatures and the newfound 150 MPa isobaric transformation temperatures concurrently allows for an initial estimation of the phase diagram. This can be seen in Fig. 2.32.

With an estimate of the phase diagram constructed, the material stabilization procedure and apparatus were designed. Further review of the intended application revealed that the maximum stresses in the beam actuators would not exceed 300 MPa. Therefore, this was chosen as an appropriate stabiliza-

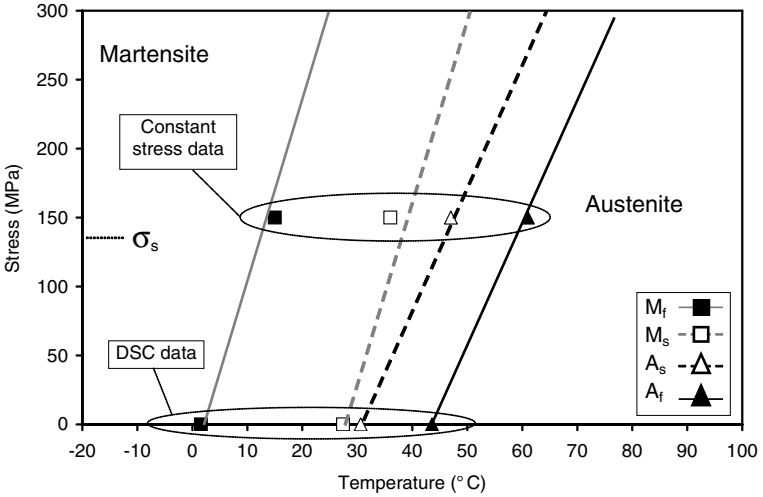

Fig. 2.32. Initial estimate of the phase diagram; Example 3, as-received material.

tion constant stress level. To complete experimental design, the approximate phase diagram was consulted, and it was determined that, for full reverse transformation into austenite at this stress level, the entirety of the specimen gauge length should be heated to $\sim 100\,^{\circ}\mathrm{C}$. A total of 100 thermal cycles at a constant stress of 300 MPa were applied while the strain response was monitored. In this case, training was performed at an accelerated rate; therefore, correct measurement of the specimen temperature was not guaranteed. However, the end goal of training is the application of multiple cycles, not the careful determination of specimen behavior. The training results are shown in Fig. 2.33a. Note that the final cycle has been darkened. For each cycle, the maximum strain represents the deformation in the martensitic state while the minimum strain represents the austenitic response. The difference can be used to derive the current maximum transformation strain per (2.3.6). Each of these three strain measures was monitored with each cycle, and their evolution is shown in Fig. 2.33b. Note how the material begins to stabilize rapidly in the first ~ 20 cycles, and then more slowly after this.

After material training, the careful characterization process was repeated. As the DSC is destructive (i.e., it requires a small portion to be cut from the sample), it was not appropriate to perform this test at this time. Also, exhibition of the pseudoelastic effect is inconsequential considering the final application. Therefore, the next goal was the determination of the functional form of $H^{cur}(\sigma)$. Multiple isobaric tests were performed at various stress levels, from 300 MPa down to 90 MPa and the results are shown in Fig. 2.34. The hysteresis height $\Delta\varepsilon$ was measured for each curve, and from these measurements $H^{cur}(\sigma_i)$ is derived via (2.3.6) (where $\sigma_1 = 300\,\mathrm{MPa}$, $\sigma_2 = 250\,\mathrm{MPa}$, etc). The

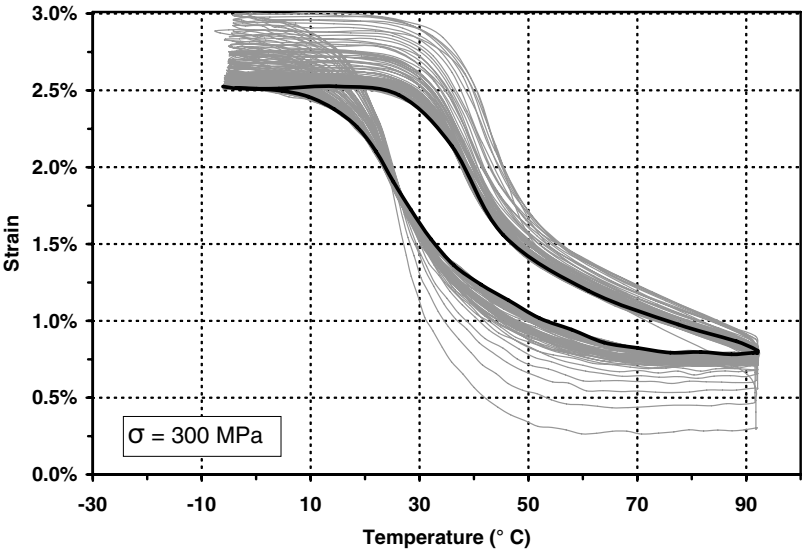

(a) Strain/temperature training cycles.

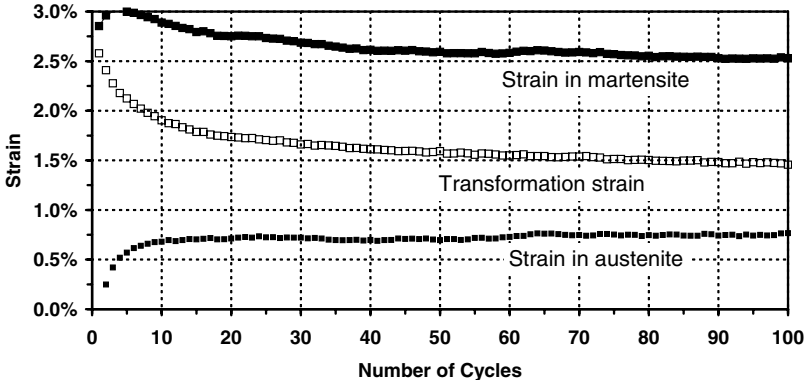

(b) Stabilization of response.

Fig. 2.33. Results of 100 applied constant stress cycles at a stress of 300 MPa; Example 3.

results for the current experimental study are shown below in Fig. 2.35 along with an analytical fit which suggests that an exponential form of $H^{cur}(\sigma)$ is appropriate.

Finally, an accurate phase diagram was determined. The transition temperatures exhibited at each constant stress applied during isobaric testing were plotted concurrently with an estimated transformation surface as shown in Fig. 2.36. The material properties determined from these experiments are

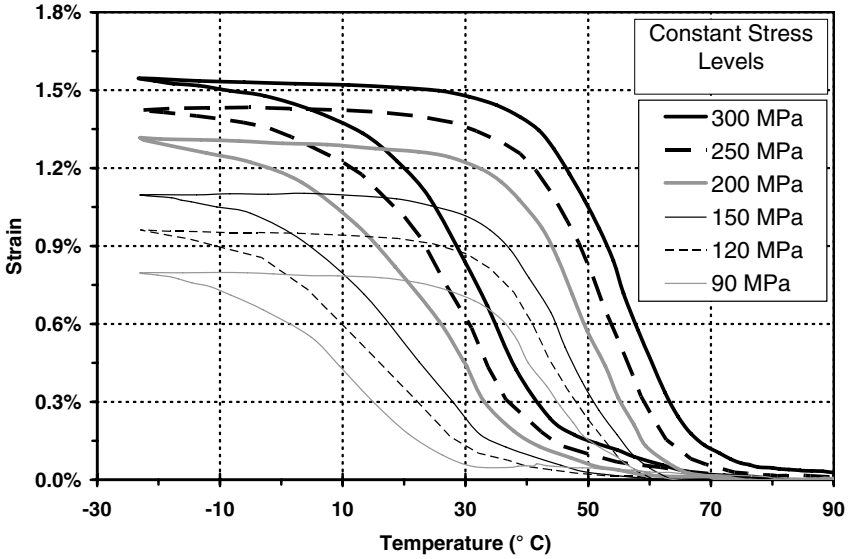

Fig. 2.34. Isobaric thermal cycling results for six applied stress levels; Example 3, trained material.

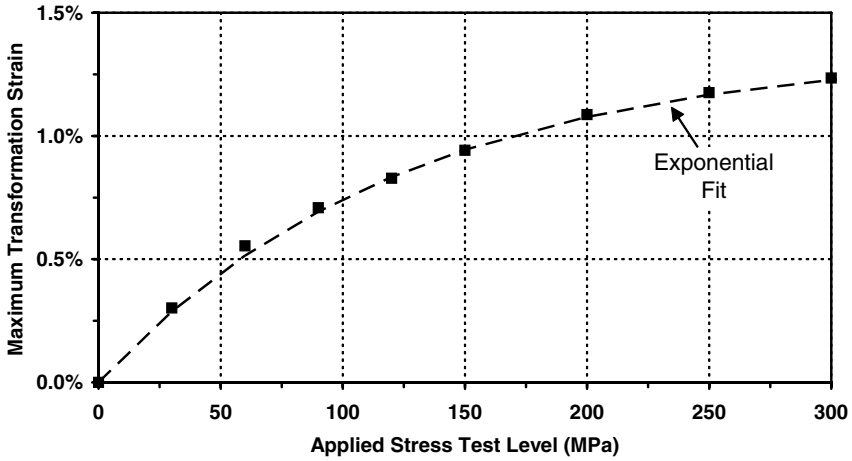

Fig. 2.35. Variation of maximum transformation strain with applied stress level; Example 3, trained material.

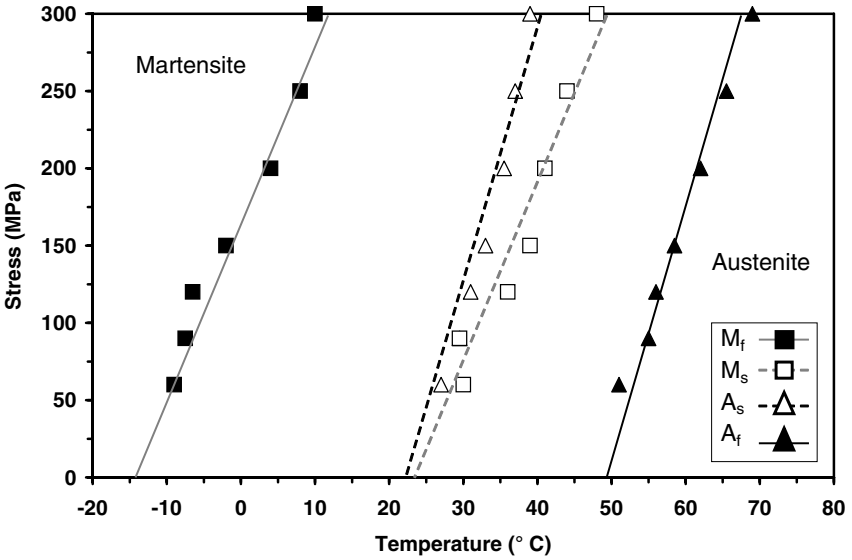

Fig. 2.36. Final experimental phase diagram derived from constant stress loading paths; Example 3, trained material.

given in Table 2.4. To graphically summarize a portion of the characterization process described in this example, Fig. 2.37 is also provided. Here is shown how bulk material (raw SMA plate) is used to construct appropriate testing specimens which are then subject to thermomechanical loading paths (cooling via liquid nitrogen spray under constant load). This subsequently leads to the generation of useful data which can be interpreted according to the methods discussed in this chapter.

Table 2.4. Experimentally derived material parameters; Example 3, trained material.

Material Parameter	Value
E^A	90 GPa
E^M	63 GPa
M_s	23 °C
M_f	−14 °C
A_s	22 °C
A_f	49 °C
C^A	16.0 MPa/ °C
C^M	11.4 MPa/ °C
$H^{cur}(\sigma)$	$= 0.0135[1 - \exp(-720\sigma/E^A)]$

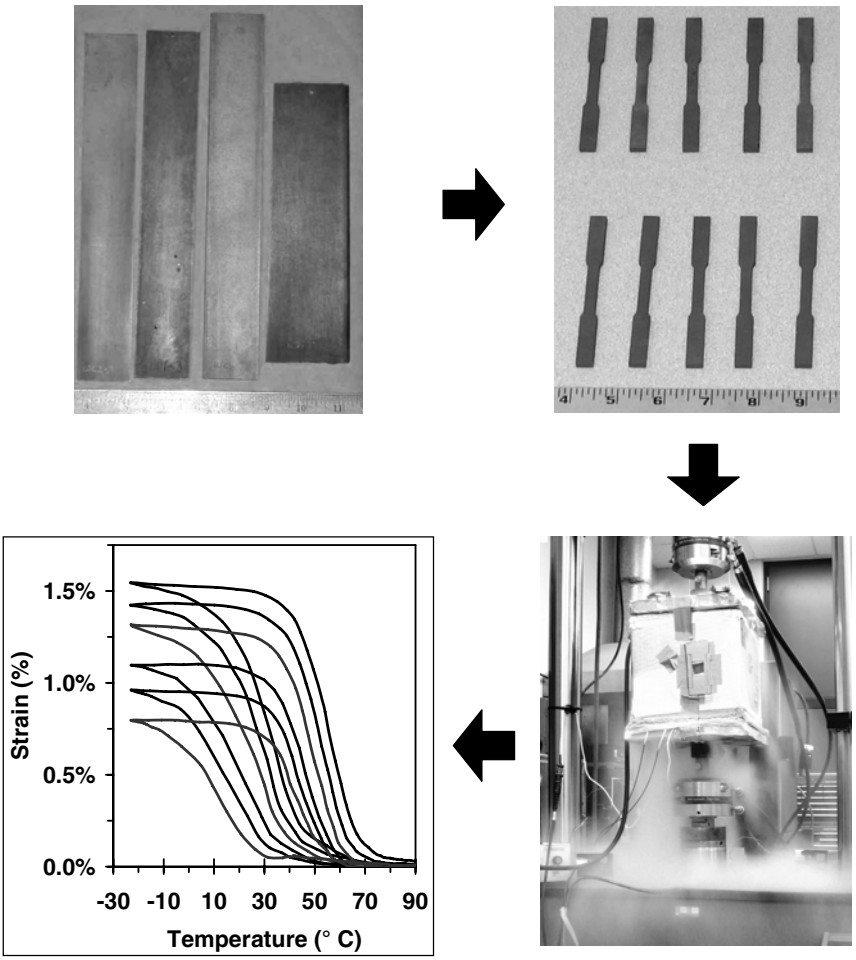

Fig. 2.37. Graphical summary of the thermomechanical characterization process as used in Example 3.

2.6 Simple SMA Application Design and Empirical 1-D Analysis

To begin the initial design of an SMA component for use in an engineering application, one must be able to choose a suitable alloy composition and then estimate the overall system response. To choose an alloy, knowledge of various required design parameters is required, and this will be discussed below. For the purposes of initial response estimation, a simple 1-D empirical model is also described in this section.

2.6.1 Application Design Considerations

The first and most fundamental step in the design of an SMA application is the determination of the operational limits. From the discussion of these first two chapters, it should be clear that important SMA behaviors are based on the current stress-temperature state and loading history. Therefore, the phase diagram represents the key design space. Using this tool, one can estimate upper and lower bounds for the operating temperature and the required stress range.

Furthermore, the limits on the maximum transformation strain for a given material should also be considered. Each of these three limit determinations are valuable in helping a designer choose a particular shape memory alloy and subsequent thermomechanical treatment for a particular set of material properties. Specifically, operation stress and temperature allow selection of the transformation temperatures, and this knowledge, combined with estimates of required actuation strain, further allow an alloy to be chosen.

Often, the most easily determined system parameter is the required operating temperature range of an active SMA component. It is estimated by considering the ambient temperature, the ability to heat the SMA element (power availability), and the ability to cool the element (via active cooling or heat conduction/convection). The operating stress range is defined by considering the SMA component loading path, especially in stress-temperature space. For example, pseudoelastic components usually undergo large variations in stress over time while some actuators may experience large temperature variations with little stress deviation.

With a stress-operating temperature envelope defined, one can now estimate the zero-stress transformation temperatures required of an SMA material for a given application. Knowledge of these temperatures is key to choosing a particular shape memory alloy. An example of such an operational envelope is given in Fig. 2.38. On a stress-temperature phase diagram, one should first identify the points $(T^{\min}, \sigma^{\min})$ and $(T^{\max}, \sigma^{\max})$. These are the estimated minimum and maximum stress and temperature states that the application is expected to apply to the installed SMA component of interest. For complete phase transformation, the maximum temperature must exceed the non-zero stress austenitic finish temperature A_f^σ as computed at maximum stress (i.e. $T^{\max} \geq A_f^\sigma,\ \sigma = \sigma^{\max}$) and likewise, during cooling ($T^{\min} \leq M_f^\sigma,\ \ \sigma = \sigma^{\min}$). Assuming a simple linear relationship between stress and temperature on the transformation lines in the phase diagram, one may then select reasonable slopes (stress influence coefficients). Values for C^A and C^M from 5 MPa/K to 10 MPa/K are generally the most reasonable. Extrapolating down to the zero-stress axis via relations (2.6.8), A_f and M_f can be found (assuming complete actuation is required).

$$A_f \leq T^{\max} - \frac{\sigma^{\max}}{C^A} \qquad M_f \geq T^{\min} - \frac{\sigma^{\min}}{C^M} \tag{2.6.8}$$

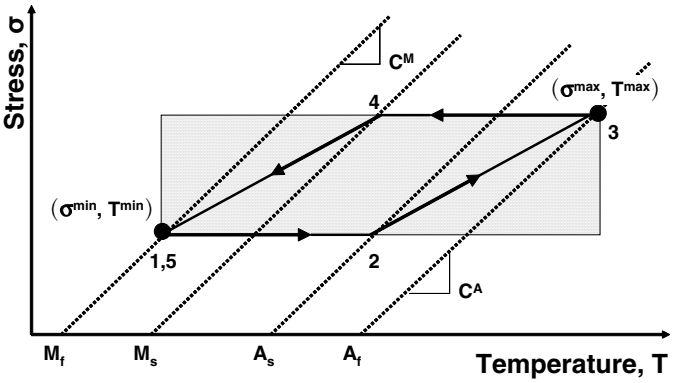

Fig. 2.38. Example of SMA application design space.

The shaded area in Fig. 2.38 designates the operating regime of the SMA actuator. A possible actuation path is shown as 1-2-3-4, point 1 being the starting point, 2 being the temperature for transformation initiation under $\sigma^{\min}$, 3 the temperature for actuation completion under $\sigma^{\max}$, and 4 being the temperature for the initiation of transformation back to the original configuration or state, 5.

The determination of the required actuation strain is the final step in determining a suitable alloy. This can be derived from the amount of mechanical motion required of a given actuator and is thus application-specific. For one-time use elements, one can effectively utilize actuation strains that are near the maximum attainable by a given alloy, i.e., up to 8% for NiTi (Sect. 1.9.1). However, for elements that are used repeatedly, lower transformation strains are favorable as they increase fatigue life and decrease plastic strain development. Considering the known operating temperature, stress and strain, it is now possible to choose an appropriate shape memory alloy. For many conventional applications, NiTi will suffice. It is both relatively affordable and widely available. However, for specialty applications, other alloys should be researched. A summary of approximate material parameters for various common SMAs, including NiTiPd for use at high temperatures, is given in Table 2.5. Recall that representative transformation temperatures were provided in Table 1.1.

For many applications using simple SMA components subject to uniform or near-uniform stress states (i.e., wires, torque tubes), one can also consider the *end states* of operation. These represent the device configurations or states at the end of forward and reverse transformation, or when the component has fully transformed in martensite and austenite. To do so requires only the use of (2.3.2) and (2.3.3), coupled with additional relations describing the operation of the device (e.g., external forces, biasing spring loads, etc.). These above equations require only the distinctive properties of pure austenite and pure martensite. We must develop a more complete material model to predict the

Table 2.5. Approximate material properties for various SMA material systems

Property	NiTi	NiTiCu	NiTiPd	CuAlNi
E^A	70 GPa	50 GPa	15 GPa	90 GPa
E^M	30 GPa	25 GPa	25 GPa	80 GPa
ν	0.3	0.3	0.3	0.3
α	$10 \cdot 10^{-6}/\,^{\circ}\mathrm{C}$	$10 \cdot 10^{-6}/\,^{\circ}\mathrm{C}$	$10 \cdot 10^{-6}/\,^{\circ}\mathrm{C}$	$15 \cdot 10^{-6}/\,^{\circ}\mathrm{C}$
C^A	7 MPa/ °C	10 MPa/ °C	5 MPa/ °C	–
C^M	7 MPa/ °C	10 MPa/ °C	5 MPa/ °C	–
H^{max}	6%	5%	3%	4%
ρ	6500 kg/m^3	6500 kg/m^3	8200 kg/m^3	7500 kg/m^3
σ^y	700 MPa	600 MPa	400 MPa	300 MPa

system response during phase transformation. A simple empirical 1-D example is derived next, and full 3-D modeling accounting for more complex material behaviors will be introduced throughout the remainder of this book.

2.6.2 Experimentally-Based 1-D Material Model

Based on the experimental results presented throughout this chapter and in Chapter 1, we can derive a simple empirical 1-D material model to capture the overall material behavior. Furthermore, we can use the material parameters discussed in this chapter and derived in the examples to calibrate such a model. Of course, for complex engineering applications of SMAs using 3-D components, such a model is not appropriate. However, it is useful for the design and analysis of applications based on SMA components undergoing homogeneous stress with only one component (i.e., uniaxial or shear stress). For simplicity, the model derived below does not account for partial transformation, which is the subject of Problem 2.10 at the end of this chapter. Additional empirical assumptions will be described as the model is derived.

Relations for the stable, fully transformed material state have already been given in (2.3.3) and (2.3.2), which follow easily from (2.3.1). Here we seek to account for 1-D material response during transformation as well. The model is derived based on the same "strength of materials" understanding of the constitutive behavior as was previously employed, and uses the *total martensitic volume fraction*, ξ, to track the progression of the phase transformation. Specifically, $\xi = 0$ when the material is fully austenitic, or in the parent phase, and $\xi = 1$ when the material is fully martensitic.

Recall Sect. 2.2.3 regarding $H^{cur}(\sigma)$ and H^{max}: a material transforming into pure detwinned martensite will exhibit the maximum attainable transformation strain, H^{max}. However, a material transforming into martensite of multiple variants will generate a recoverable strain that depends on stress, $H^{cur}(\sigma)$. In this model, and in all models presented in Chapters 3–6, ξ will denote the *total martensitic volume fraction*, which may include multiple variants (fully twinned, fully detwinned, or some combination). Because H^{max} is

exhibited when only pure detwinned martensite is present, we can also define a relation that gives the *detwinned martensitic volume fraction* as:

$$\xi^d = \frac{H^{cur}(\sigma)}{H^{max}}\xi \tag{2.6.9}$$

Of course it is straightforward to see that we could also give the *twinned martensitic volume fraction* as:

$$\xi^t = \xi - \xi^d = \frac{H^{max} - H^{cur}(\sigma)}{H^{max}}\xi \tag{2.6.10}$$

To continue, only ξ is considered and the following three assumptions are made:

- **Assumption 1:** The elastic stiffness, unique for each phase, varies linearly with varying martensitic volume fraction. This is consistent with a *rule of mixtures* approach to accounting for austenitic and martensitic elastic stiffness. In more complex models, other relations employing the methods of micromechanics are sometimes used.

$$E = E^A + \xi(E^M - E^A) \tag{2.6.11}$$

- **Assumption 2:** The coefficient of thermal expansion (α) is a constant.
- **Assumption 3:** The 1-D transformation strain varies linearly with varying total martensitic volume fraction such that:

$$\varepsilon^t = \xi H^{cur}(\sigma) \tag{2.6.12}$$

Note that the sign of H^{cur} is dependent on the particular stress applied (i.e., $H^{cur} \geq 0$ for tensile stress, $H^{cur} \leq 0$ for compressive stress). Substituting these two relations into (2.3.1) yields:

$$\sigma = [E^A + \xi(E^M - E^A)][\varepsilon - \xi H^{cur}(\sigma) - \alpha(T - T_0)] \tag{2.6.13}$$

To further capture transformation behavior, it is necessary to use the phase diagram that captures the critical 1-D stress and temperature states at which transformation is induced and completed. From observation of the numerous phase diagram examples shown throughout the chapter, the following assumption is inferred:

- **Assumption 4:** The transformation start and finish temperatures at a given stress (e.g., M_s^σ and A_f^σ) are linearly related to the applied stress. This implies the following relations:

$$M_s^\sigma = M_s + \frac{\sigma}{C^M} \tag{2.6.14}$$

$$M_f^\sigma = M_f + \frac{\sigma}{C^M} \tag{2.6.15}$$

$$A_s^\sigma = A_s + \frac{\sigma}{C^A} \tag{2.6.16}$$

$$A_f^\sigma = A_f + \frac{\sigma}{C^A} \tag{2.6.17}$$

To complete the 1-D empirical model, the evolution of martensitic volume fraction with changing stress-temperature state must be addressed. A final assumption is then required.

- **Assumption 5:**
  - During *forward transformation*, the martensitic volume fraction, ξ, linearly increases with decreasing temperature from M_s^σ to M_f^σ. Because $M_s^\sigma - M_f^\sigma = M_s - M_f$, this can be written as:

$$\xi = \frac{M_s^\sigma - T}{M_s - M_f} \tag{2.6.18}$$

  - During *reverse transformation*, the martensitic volume fraction, ξ, linearly decreases with increasing temperature from A_s^σ to A_f^σ. Because $A_f^\sigma - A_s^\sigma = A_f - A_s$, this can be written as:

$$\xi = \frac{A_f^\sigma - T}{A_f - A_s} \tag{2.6.19}$$

This is schematically illustrated in Fig. 2.39 where forward transformation is shown in Fig. 2.39a and reverse transformation in Fig. 2.39b. Note that this assumption on the evolution of ξ is applicable regardless of the arbitrary loading path experienced by the SMA material. Whenever the stress-temperature state is within the transformation region, the current transformation temperatures at given (non-zero) stress can always be calculated via (2.6.14)–(2.6.17).

Assumption 5 combined with previous assumptions allows us to define the martensitic volume fraction for all points on the phase diagram when

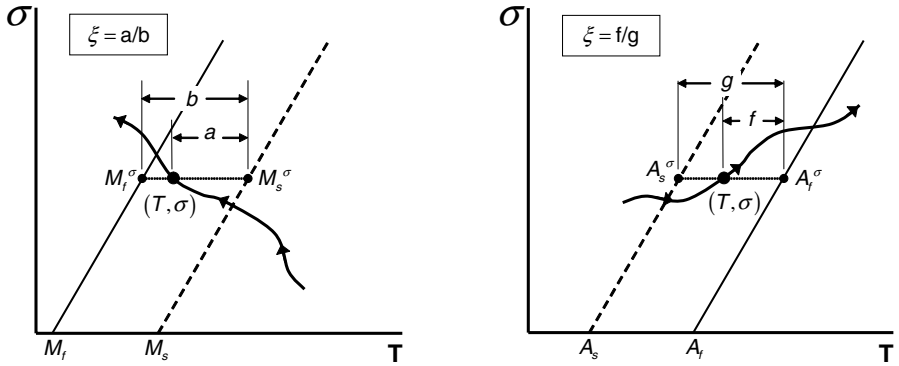

(a) Forward transformation. (b) Reverse transformation.

Fig. 2.39. Schematic illustrating the assumed transformation behavior for the evolution of martensitic volume fraction.

cooling/loading into martensite and when heating/loading into austenite. The relations for ξ are given below where (2.6.14) and (2.6.17) are substituted into (2.6.18) and (2.6.19), respectively.

For *loading/cooling into martensite*, the martensitic volume fraction is given as:

$$\xi = \begin{cases} 0, & T \geq M_s^\sigma, \\ \dfrac{M_s + \dfrac{\sigma}{C^M} - T}{M_s - M_f}, & M_f^\sigma < T < M_s^\sigma, \\ 1, & T \leq M_f^\sigma, \end{cases} \tag{2.6.20}$$

while for *loading/heating into austenite* is given as:

$$\xi = \begin{cases} 1, & T \leq A_s^\sigma, \\ \dfrac{A_f + \dfrac{\sigma}{C^A} - T}{A_f - A_s}, & A_s^\sigma < T < A_f^\sigma, \\ 0, & T \geq A_f^\sigma. \end{cases} \tag{2.6.21}$$

Using (2.6.13) combined with either (2.6.20) or (2.6.21), as appropriate, there are sufficient relations to describe the 1-D SMA behavior during both transformation ($0 < \xi < 1$) and thermoelastic loading ($\xi = 0$ or $\xi = 1$). Recall that this model in its current form does not account for partial transformation.

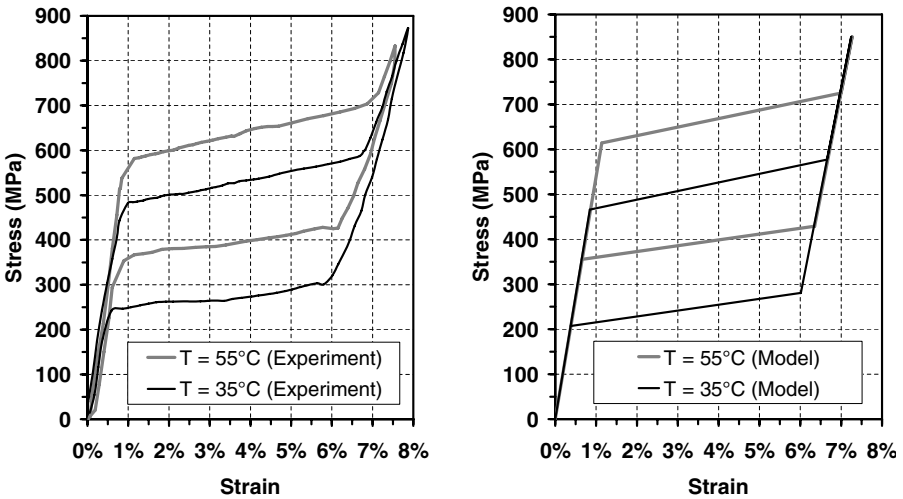

(a) Experiment (b) Empirical model

Fig. 2.40. Comparison of experimental pseudoelastic results and 1-D empirical model predictions (cf. Example 1, Sect. 2.5.1).

This model has been used to present the pseudoelastic results shown in the first example in Sect. 2.5.1. The material properties used to calibrate the model are given in Table 2.2. Here (Fig. 2.40) the isothermal responses at 35 °C and 55 °C are shown, and the model accurately captures the material behavior.

Finally, note that the 1-D relations given above can be re-written for homogeneous shear. Several engineering applications of SMAs utilize shear deformation, and many of these include torque tube components. For sufficiently thin SMA torque tubes, the variation in stress and strain through the wall thickness is small enough to be negligible. For the design of such applications, it is advantageous to utilize an analytical model such as that given above to approximate the actuation behavior. This requires that the relations above be rewritten for shear, where, for example τ and γ denote shear stress and strain, respectively, and $\gamma = 2\epsilon_{12}$. For such a model, material calibration should be formed using experimental data taken from shear loading.

2.7 Summary

Understanding the experimental characterization of shape memory alloys is important not only for those who plan to quantify material properties, but also for those analysts and designers who must form a solid understanding of SMA behavior. As with characterization of any material, known inputs are applied and exhibited outputs are monitored and evaluated. As one becomes more familiar with the uncommon properties of shape memory alloys, an intuition into the material response to a given thermomechanical load is formed. An understanding of the simple 1-D phenomenological response allows the construction of empirical material models, as exemplified above. As this understanding grows, the formulation and refinement of more advanced theoretical models that explain or even predict more complicated behavior becomes possible.

Furthermore, once a model has been proposed, numerical implementation is necessary to convert a theory into a useable tool for the design and analysis of engineering applications. The formulation and calibration of various models and their numerical implementation will be the topic of the remainder of this book.

2.8 Problems

2.1. Recall that the determination of the stress-free transformation temperatures A_s and A_f can be performed using either DSC or free bend recovery. How might the temperatures determined by these two methods differ? What would cause such a difference?

2.2. Describe two other methods by which all four stress-free transformation temperatures could be experimentally determined and which does not involve the measurement of heat flow (i.e., DSC) or deformations (i.e., bend and free recovery).

2.3. In the experimental work performed by Shaw and Kyriakides [12], a fluid bath was employed for most isothermal tests. Why was such an experimental setup used? Explain the consequences of using an ambient air environment instead.

2.4. Consider further the experimental work performed by Shaw and Kyriakides [12]. Explain the mechanisms that lead to the significant variation in "strain" as measured via crosshead displacement ($\Delta l/l_0$) vs. measurement by locally-mounted extensometers (ε) (see "Figure 12d" in the referenced work).

2.5. Consider the isothermal stress-strain experimental results shown in Fig. 2.6b. From these results, determine appropriate material parameters. Assume material isotropy.

a) Determine the elastic stiffnesses of the material.
b) Construct the phase diagram for this material configuration.
c) Determine a suitable maximum transformation strain. Does the amount of transformation strain generated during forward transformation vary significantly with increasing upper plateau stress level?

2.6. Consider the constant stress experimental results shown in Fig. 2.41. From these results, determine the material parameters assuming material isotropy.

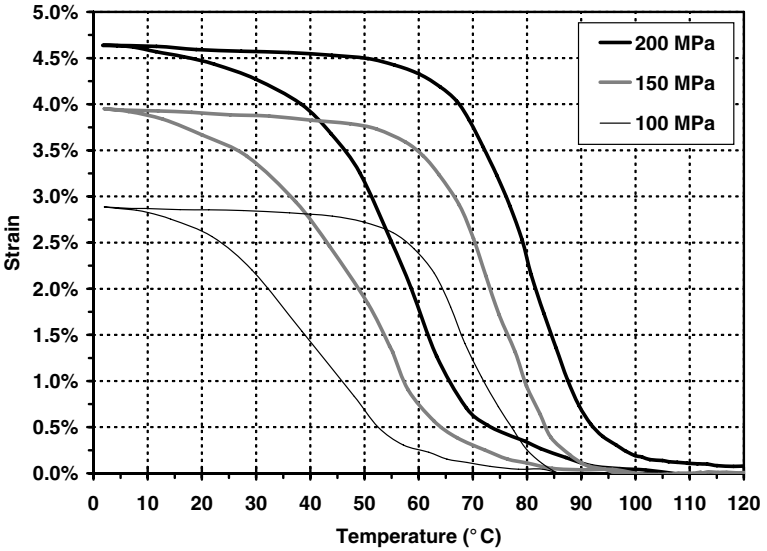

Fig. 2.41. Example of isobaric strain-temperature experimental results for near-equiatomic NiTi.

a) Use the elastic properties from Problem 2.5.
b) Construct the phase diagram for this material configuration.
c) Determine a suitable function to describe the maximum transformation strain at all effective stress levels.

2.7. Consider the experimental work performed and reported by Miyazaki et al. [7].

a) Using the data in "Fig. 1" from this reference, reconstruct and complete the phase diagram shown in "Fig. 2" (i.e., add the transformation *finish* surfaces).
b) Based on this phase diagram, approximate three distinct strain-temperature cyclic responses if this material is subjected to full thermal cycles at three distinct constant stresses.

2.8. Determine the three thermomechanical states (i.e., stress-strain-temperature states) of an SMA wire with a length of 0.5 m and a diameter of 0.25 mm if it is initially unstressed at $T = -10\,°\text{C}$ (Point 1), then subjected to a constant load of 15 N at $-10\,°\text{C}$ (Point 2), then heated to 150 °C (Point 3). Sketch these points and the connecting paths on the phase diagram, on a stress-strain plot, and on a strain-temperature plot.

a) Use the material properties from Problem 2.5.
b) Use the material properties from Problem 2.6.

2.9. Determine the three equilibrium states of the SMA wire from Problem 2.8 if it is initially unstressed, then placed in opposition to an elastic spring with a spring constant of 4 N/mm with a prestress of 75 MPa at $-10\,°\text{C}$, then heated to 150 °C. Sketch these paths on the phase diagram and on a stress-strain plot.

a) Use the material properties from Problem 2.5.
b) Use the material properties from Problem 2.6.

2.10. Repeat Problem 2.8 using the simple 1-D model derived in Sect. 2.6.2. Specifically, derive and plot the continuous analytical solution of the wire stress-strain response. (*Hint: The solution must be determined incrementally to account for the beginnings/endings of transformation.*)

2.11. Consider the case in which two SMA rods are arranged as shown in Fig. 2.42 where both rods exhibit the material properties from Problem 2.5. The cool wire is assumed to be initially fully detwinned and the initial tensile stress level in both rods is given.

a) If rod 1 is heated from T_0 to T_f, and then cooled back to T_0, determine the thermomechanical states (stress, strain, and temperature) at the end of heating and at the end of cooling. Plot these two points on an approximate quantitative phase diagram.
b) Repeat the case where the temperature of rod 2 is a constant 100 °C.

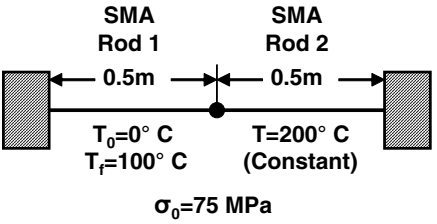

Fig. 2.42. SMA rods in an "antagonistic" configuration.

(*Hint: The solution must be determined incrementally using the model in Sect. 2.6.2.*)

2.12. For the simple 1-D model presented in Sect. 2.6.2, add the necessary relations to account for partial transformation. Model a case of isothermal loading at $T = 40\,^{\circ}\mathrm{C}$ using the material parameters given in Table 2.2. Load the material such that ξ reaches a value of 0.5, and then unload. At what stress does ξ reach 0.5? At what stress state should reverse transformation begin? (*Hint: Consider reformulating 2.6.21 considering that ξ must be continuous.*)

2.13. An SMA wire has length $2L$, diameter D, and maximum transformation strain $H^{cur} = H^{max}$. It is initially in a twinned martensitic state and is installed between two rigid supports in a stress-free, straight configuration. A weight W sufficient to induce and complete detwinning is then hung on the wire. This configuration is shown in Fig. 2.43. Assuming that $E^A = E^M$, determine the initial angle θ_i just after the weight is added. Furthermore, determine the elevation, e, of the weight when the wire becomes fully austenitic upon heating. For the case of $E^A \neq E^M$, find the new elevation and compare its percent difference with respect to the previous case. For this problem you may neglect any influence of thermal expansion and the weight of the wire itself.

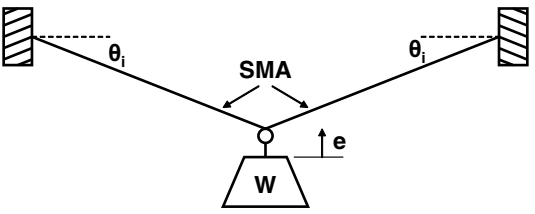

Fig. 2.43. Weight suspended from an SMA wire.

2.14. Consider a composite cylinder as shown in Fig. 2.44, formed by first expanding a martensitic SMA cylinder to an inner radius R through a detwinning process which causes a tangential transformation strain of $\varepsilon_\theta^t = 0.03$. The

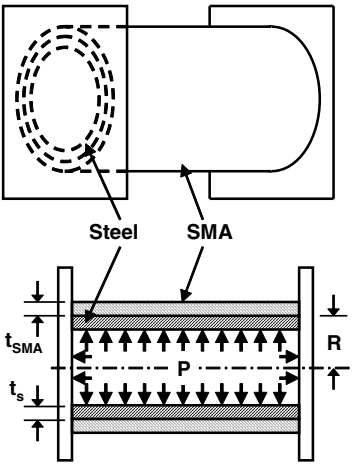

Fig. 2.44. SMA/steel composite cylinder of radius R and subjected to internal pressure P.

SMA cylinder is then brought over a steel cylinder of outer radius R. Assume that the thicknesses of both cylinders are very small compared to their radius (i.e., $t_{SMA} \ll R$ and $t_s \ll R$). The composite cylinder is pressurized by an internal pressure, P, while it is held between two rigid surfaces that allow only radial expansion or contraction but not any axial deformation. The composite cylinder is then subjected to a uniform temperature change, sufficient to cause 90% phase transformation of the SMA from detwinned martensite to austenite, while small enough to neglect any thermal expansion mismatch effects. Determine the stress in both the steel and the SMA cylinders for the case $t_s = t_{SMA} = 0.03R$. Assume also that $E_s = 200\,\text{GPa}$, $\nu_s = 0.3$; $E_{SMA} = 30\,\text{GPa}$, $\nu_{SMA} = 0.3$ (Both austenite and martensite elastic properties are assumed to be the same).

2.15. Describe the feasibility of the following SMA/SMA antagonistic actuator composed of two concentric cylinders. Assume that the inner SMA cylinder is prestrained axially until $\varepsilon^t = 0.056$ and then relaxed at $T < A_s$, at which time it is equal in length to the outer SMA cylinder. The outer cylinder, also at $T < A_s$, remains in a twinned martensite state ($\varepsilon^t = 0$). The actuator is assembled at a temperature below A_s and this assembly is shown below in Fig. 2.45 in the stress-free configuration. The actuator length $L = 150\,\text{mm}$ and the cross-sectional area is $50\,\text{mm}^2$ for both SMA cylinders. Use SMA properties from Table 2.2. Assume that when the inner SMA cylinder is heated above A_s, the outer remains at a temperature below A_s.

a) By assuming a uniaxial stress state in the cylinder assembly, find the maximum actuation force that the actuator can generate (actuator "blocking force") as the temperature of the inner cylinder is raised to A_f.

b) Determine the stroke of the actuator for actuation force of 10% of the blocking force.

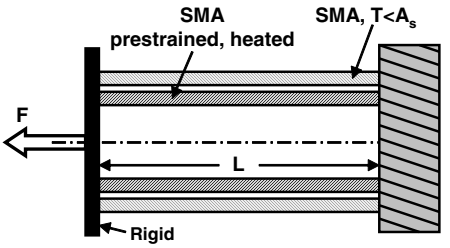

Fig. 2.45. SMA/SMA concentric cylinder antagonistic actuator.

2.16. Consider the cyclic response of an SMA-linear antagonistic actuator, shown in Fig. 2.46, under temperature variations. Use SMA properties for NiTi from Table 2.5. The length of both SMA bars is 150 mm and their cross-section is 25 mm^2. The initial state of the SMA actuators is martensitic with the left SMA prestrained to $\varepsilon^t = 0.06$. The initial assembly of the antagonistic actuation system is such that each SMA component is stress free. An SMA thermal history will be considered whereby the temperature of a component is heated from its initial temperature $T_0 < A_s$ to a maximum temperature of $T_{max} = A_s + 50\,°C$ and then cooled to $T_{min} = M_s - 50\,°C$.

a) Determine the actuator system blocking force F_{block} by finding the maximum force when point A is constrained (zero displacement) while the left SMA actuator is heated to T_{max}.
b) Consider the following heat/cool cycle: the right actuator, which is initially in a unstressed twinned martensite state, remains at T_0 while the left SMA actuator is heated to T_{max} and then cooled to T_{min}, after which the right actuator is heated to T_{max} and then cooled to T_{min}. This heating/cooling cycle is alternately applied to the right and left actuators until the system response stabilizes. Assuming $F = 0.5F_{block}$, determine the cyclic response of the actuator by plotting the displacement of point A with respect to temperature for several temperature cycles until a repeatable actuation path is reached.

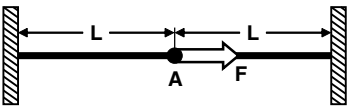

Fig. 2.46. SMA linear antagonistic actuator.

c) Discuss the advantages and disadvantages of this form of antagonistic actuator when compared to the configuration described in Prob. 2.15.

2.17. Figure 2.47 shows an SMA-powered automobile designed and constructed by freshmen engineering students at Texas A&M University. This vehicle uses a "10-cylinder" NiTi SMA engine as opposed to a conventional internal combustion engine.

The SMA wires have material properties as given for NiTi in Table 2.5. The 10 wires are each prestrained to $\varepsilon^t = 0.06$ prior to installation on the automobile and the bias springs, once attached, apply a nearly constant force resulting in a stress of 150 MPa. The diameter of the wires is 0.15 mm and their length is 80 mm. The repeating process of "firing" all 10 SMA pistons is assumed to take 10 seconds per cycle, with each wire heated independently and for an equal amount of time to $T_{max} = 80\,^{\circ}\mathrm{C} > A_f^{\sigma}$. Cooling is convective and $T_{min} = 30\,^{\circ}\mathrm{C} < M_f^{\sigma}$. The duty cycle for each wire is 10% heating, 90% cooling. The electrical resistivity of the SMA material is $80\,\mu\Omega$-cm, the latent heat of transformation is $20\,\mathrm{J\text{-}g^{-1}}$, and the heat capacity is $0.32\mathrm{J\,^{\circ}C^{-1}g^{-1}}$. The car is powered by a 9 V battery.

a) Find the horsepower of this SMA automobile engine. Estimate its efficiency as a "green" electric car.
b) What would be the required cross-sectional area of 10 SMA wires (or rods), each with a length of 1.0 m, to design a 100 HP engine? How much electric power would be required to operate such an SMA engine?

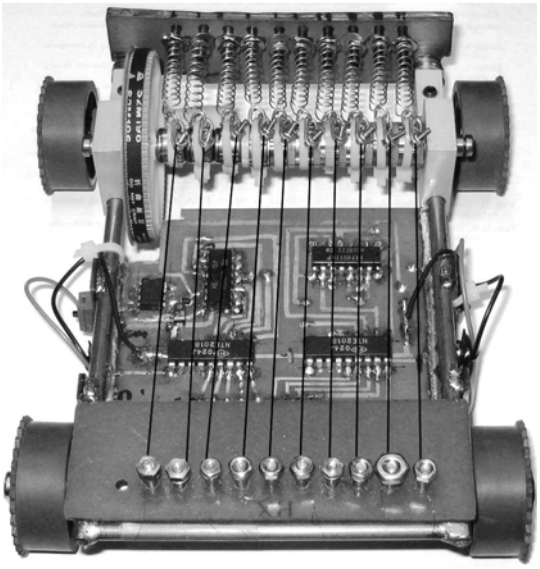

Fig. 2.47. SMA-powered 10 "cylinder" automobile (SMA wires accentuated for clarity).

2.18. Consider the SMA-actuated grippers shown in Fig. 2.48 (where all dimensions are given in mm). A single NiTiCu SMA wire with a diameter of 0.6 mm and properties as given in Table 2.5 is attached to the gripper at two locations, one on each jaw. The attachment points are shared with a bias spring that has a spring constant of $k = 0.5\,\mathrm{N/mm}$. The SMA wire also passes over three pulleys: two are symmetric and adjustable and the third is located on the gripper axis of symmetry. Before installation in a stress free state (grips closed), the SMA wire is prestrained to 5% transformation strain. The preload in the spring when the grips are closed is 25 N.

Moving outward from the centerline, the first adjustable pulley position is located 40 mm from the centerline of the grippers. Five additional possible positions are spaced 10 mm apart along a line perpendicular to the centerline (see Fig. 2.48).

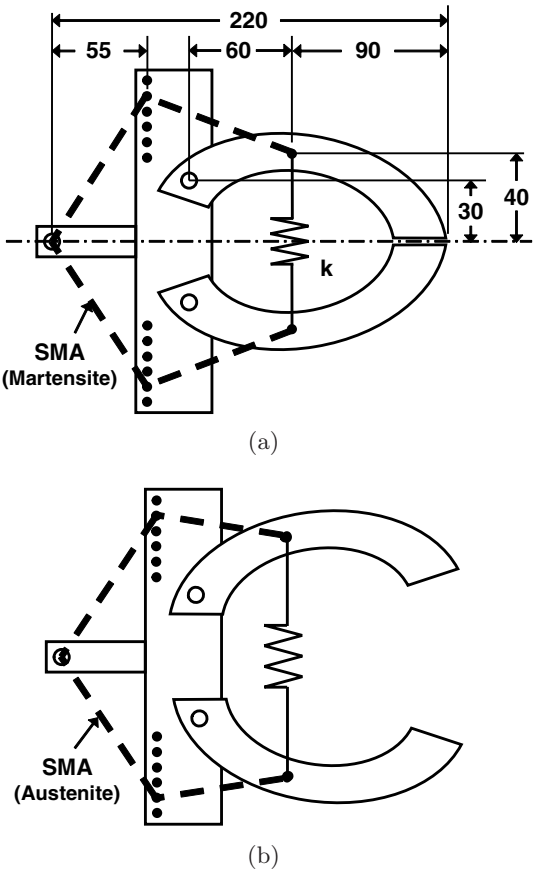

Fig. 2.48. SMA gripper as discussed in Problem 2.18 (all dimensions in mm); a) closed configuration; b)open configuration.

Determine the optimal symmetric pulley position such that the opening motion of the grips is maximized when the SMA is heated into full austenite. Do not allow the SMA stress to exceed 70% of the yield stress. Repeat for the case where the spring constant is doubled to 1.0 N/mm. Repeat once more if the preload on the spring is 50 N. How could this design be improved if there were no constraints on the location of the symmetric pulleys?

References

[1] W. Buehler, R. Wiley, The properties of TiNi and associated phases, Tech. rep., U.S. Naval Ordnance Laboratory (1961).

[2] C. M. Jackson, H. J. Wagner, R. J. Wasilewski, 55-Nitinol—The alloy with a memory: Its physical metallurgy, properties and applications, Tech. Rep. NASA SP-5110, NASA Technology Utilization Office, Washington, D.C. (1972).

[3] K. Otsuka, C. M. Wayman (Eds.), Shape Memory Materials, Cambridge University Press, Cambridge, 1999.

[4] J. Perkins, Shape Memory Effects in Alloys, Plenum Press, New York, 1975.

[5] H. Funakubo (Ed.), Shape Memory Alloys, Gordon and Breach Science Publishers, 1987.

[6] X. Ren, K. Otsuka, Universal symmetry property of point defects in crystals, Physical Review Letters 85 (5) (2000) 1016–1019.

[7] S. Miyazaki, K. Otsuka, Y. Suzuki, Transformation pseudoelasticity and deformation behavior in a Ti-50.6at%Ni alloy, Scripta Materialia 15 (1981) 287–292.

[8] Z. Bo, D. C. Lagoudas, Thermomechanical modeling of polycrystalline SMAs under cyclic loading, Part I: Theoretical Derivations, International Journal of Engineering Science 37 (1999) 1089–1140.

[9] D. C. Lagoudas, Z. Bo, Thermomechanical modeling of polycrystalline SMAs under cyclic loading, Part II: Material characterization and experimental results for a stable transformation cycle, International Journal of Engineering Science 37 (1999) 1141–1173.

[10] Z. Bo, D. C. Lagoudas, Thermomechanical modeling of polycrystalline SMAs under cyclic loading, Part III: Evolution of plastic strains and two-way shape memory effect, International Journal of Engineering Science 37 (1999) 1175–1203.

[11] Z. Bo, D. C. Lagoudas, Thermomechanical modeling of polycrystalline SMAs under cyclic loading, Part IV: Modeling of minor hysteresis loops, International Journal of Engineering Science 37 (1999) 1205–1249.

[12] J. Shaw, S. Kyriakides, Thermomechanical aspects of NiTi, Journal of the Mechanics and Physics of Solids 43 (8) (1995) 1243–1281.

[13] T. Duerig, K. Melton, D. Stockel, C. Wayman (Eds.), Engineering Aspects of Shape Memory Alloys, Butterworth-Heinemann, London, 1990.
[14] ASTM International, Standard Terminology for Nickel-Titanium Shape Memory Alloys (2005).
[15] ASTM International, Standard Specification for Wrought Nickel-Titanium Shape Memory Alloys for Medical Devices and Surgical Implants (2005).
[16] ASTM International, Standard Test Method for Transformation Temperature of Nickel-Titanium Alloys by Thermal Analysis (2005).
[17] ASTM International, Standard Test Method for Determination of Transformation Temperature of Nickel-Titanium Shape Memory Alloys by Bend and Free Recovery (2003).
[18] ASTM International, Standard Test Method for Tension Testing of Nickel-Titanium Superelastic Materials (2006).
[19] ASTM International, Standard Test Method for Tension Testing of Metallic Materials (2004).
[20] H. Sehitoglu, I. Karaman, R. Anderson, X. Zhang, K. Gall, H. J. Maier, Y. Chumlyakov, Compressive response of NiTi single crystals, Acta Materialia 48 (13) (2000) 3311–3326.
[21] H. Sehitoglu, I. Karaman, X. Y. Zhang, H. Kim, Y. I. Chumlyakov, H. J. Hans Maier, I. Kireeva, Deformation of NiTiCu single crystals in compression, Metallurgical and Material Transactions A 32 (2001) 477–489.
[22] ASTM International, Standard Test Methods of Compression Testing of Metallic Materials at Room Temperature (2000).
[23] J. T. Lim, D. L. McDowell, Mechanical behavior of a Ni-Ti shape memory alloy under axial-torsional proportional and nonproportional loading, Journal of Engineering Materials and Technology 121 (1999) 9–18.
[24] A. Keefe, G. Carman, Thermo-mechanical characterization of shape memory alloy torque tube actuators, Smart Materials and Structures 9 (2000) 665–672.
[25] K. Otsuka, X. Ren, Physical metallurgy of Ti–Ni-based shape memory alloys, Progress in Materials Science 50 (2005) 511–678.
[26] E. Patoor, D. C. Lagoudas, P. B. Entchev, L. C. Brinson, X. Gao, Shape memory alloys, Part I: General properties and modeling of single crystals, Mechanics of Materials 38 (5–6) (2006) 391–429.
[27] D. C. Lagoudas, P. B. Entchev, P. Popov, E. Patoor, L. C. Brinson, X. Gao, Shape memory alloys, Part II: Modeling of polycrystals, Mechanics of Materials 38 (5–6) (2006) 430–462.
[28] B. Chang, J. Shaw, M. Iadicola, Thermodynamics of shape memory alloy wire: Modeling, experiments, and application, Continuum Mechanics and Thermodynamics 18 (1–2) (2006) 83–118.
[29] C. Lexcellent, J. Rejzner, Modeling of the strain rate effect, creep, and relaxation of a Ni-Ti shape memory alloy under tension (compression)-

torsional proportional loading in the pseudoelastic range, Smart Materials and Structures 9 (2000) 613–621.

[30] Y. Liu, Y. Li, K. Ramesh, Rate dependence of deformation mechanisms in a shape memory alloy, Philosophical Magazine A 82 (12) (2002) 2461–2473.

[31] P. Popov, K. Ravi-Chandar, D. Lagoudas, Dynamic loading of polycrystalline shape memory alloy rods, Mechanics of Materials 35 (7) (2003) 689–716.

[32] J. Nemat-Nasser, W. Choi, G. Guo, J. Isaacs, Very high strain-rate response of a NiTi shape-memory alloy, Mechanics of Materials 37 (2–3) (2005) 287–298.

[33] J. Escobar, R. Clifton, On pressure-shear plate impact for studying the kinetics of stress-induced phase transformations, Material Science & Engineering A 170 (1993) 125–142.

[34] P. Feng, Q. Sun, Experimental investigation on macroscopic domain formation and evolution in polycrystalline NiTi microtubing under mechanical force, Journal of the Mechanics and Physics of Solids 54 (8) (2006) 1568–1603.

[35] D. A. Miller, D. C. Lagoudas, Thermo-mechanical characterization of NiTiCu and NiTi SMA actuators: Influence of plastic strains, Smart Materials and Structures 9 (5) (2000) 640–652.